

NASA TECHNICAL NOTE



NASA TN D-5584

2.1

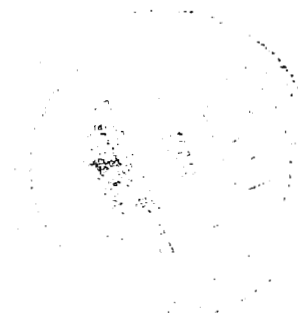
NASA TN D-5584



LOAN COPY: RETURN TO
AFWL (WLOL)
KIRTLAND AFB, N MEX

LONGITUDINAL AND LATERAL SPECTRA
OF TURBULENCE IN THE
ATMOSPHERIC BOUNDARY LAYER

by
George H. Fichtl
George C. Marshall Space Flight Center
and
George E. McVehil
Cornell Aeronautical Laboratory, Inc.





0132350

1. Report No. NASA TN D-5584		2. Government Accession No.		3. Recipient's Catalog No.	
4. Title and Subtitle Longitudinal and Lateral Spectra of Turbulence in The Atmospheric Boundary Layer				5. Report Date February 1970	
				6. Performing Organization Code	
7. Author(s) George H. Fichtl and George E. McVehil				8. Performing Organization Report No. M149	
9. Performing Organization Name and Address George C. Marshall Space Flight Center Marshall Space Flight Center, Alabama 35812				10. Work Unit No. 933-50-02-00-62	
				11. Contract or Grant No.	
12. Sponsoring Agency Name and Address National Aeronautics and Space Administration Washington, D.C. 20546				13. Type of Report and Period Covered Technical Note	
				14. Sponsoring Agency Code	
15. Supplementary Notes Prepared by the Aero-Astrodynamic Laboratory, Science and Engineering Directorate					
16. Abstract An engineering spectral model of turbulence is developed with horizontal wind observations obtained at the NASA 150-meter meteorological tower at Cape Kennedy, Florida. Spectra, measured at six levels, are collapsed at each level with $(nS(n)/u_{*o}^2, f)$ - coordinates, where $S(n)$ is the longitudinal or lateral spectral energy density at frequency $n(\text{Hz})$, u_{*o} is the surface friction velocity, and $f = nz/\bar{u}$, \bar{u} is the mean wind speed at height z . A vertical collapse of the dimensionless spectra is produced by assuming they are shape invariant in the vertical. An analysis of the logarithmic spectrum in the inertial subrange, at the 18-meter level, implies that the local mechanical and buoyant production rates of turbulent kinetic energy are balanced by the local dissipation and energy flux divergence, respectively.					
17. Key Words Structure of Atmospheric Turbulence, Turbulent Kinetic Energy, Monin Coordinates, Surface Friction Velocity				18. Distribution Statement Unclassified - Unlimited	
19. Security Classif. (of this report) Unclassified		20. Security Classif. (of this page) Unclassified		21. No. of Pages 52	22. Price* \$3.00



TABLE OF CONTENTS

	Page
SUMMARY	1
INTRODUCTION.	2
THE NASA 150-m METEOROLOGICAL TOWER.	3
Terrain Features	3
Instrumentation	6
Surface Roughness Length (z_0).	6
COMPUTATIONS AND INITIAL SCALING.	7
THE INERTIAL SUBRANGE AND REVISED VALUES OF THE SURFACE ROUGHNESS LENGTHS.	11
EXTRAPOLATION TO NEUTRAL WIND CONDITIONS ($Ri = 0$).	18
The Longitudinal Spectrum.	20
The Lateral Spectrum.	24
UNSTABLE SPECTRA.	25
THE LONGITUDINAL AND LATERAL CORRELATION FUNCTIONS . . .	27
THE DISSIPATION RATE OF TURBULENCE.	35
VERTICAL VARIATION OF STRESS IN NEUTRAL AIR.	38
CONCLUDING COMMENTS	40
REFERENCES.	42

LIST OF ILLUSTRATIONS

Figure	Title	Page
1.	The relationship between the quasi-steady and the instantaneous wind vectors and the longitudinal and lateral components of turbulence	3
2.	NASA Launch Complex 39, Kennedy Space Center, Florida,	4
3.	Aerial view of the terrain surrounding the NASA 150-m meteorological tower,	5
4.	Location of instrumentation on the NASA 150-m meteorological tower at Kennedy Space Center, Florida,	6
5.	Tentative azimuthal distribution of the surface roughness length at the NASA 150-m meteorological tower site	7
6.	The dimensionless logarithmic longitudinal spectrum at $f = 1.0$ and $z = 18$ m as a function of $-Ri$	15
7.	Revised azimuthal distribution of the surface roughness length based upon energy budget considerations at $z = 18$ m,	17
8.	Dimensionless logarithmic longitudinal spectra for neutral wind conditions	19
9.	Dimensionless logarithmic lateral spectra for neutral wind conditions	20
10.	Vertical distributions of the dimensionless frequencies f_{μ} and f_{mv} associated with the peaks of the logarithmic longitudinal and lateral spectra for neutral stability conditions	21

LIST OF ILLUSTRATIONS (Concluded)

Figure	Title	Page
11.	Vertical distributions of the collapsing factors β_u and β_v for neutral stability conditions	22
12.	Dimensionless logarithmic longitudinal and lateral spectra as functions of $0.03 f/f_{mu}$ and $0.1 f/f_{mv}$ for neutral stability conditions	23
13.	Dimensionless logarithmic longitudinal spectra for unstable wind conditions	26
14.	Dimensionless logarithmic lateral spectra for unstable wind conditions	26
15.	Vertical distributions of the dimensionless frequencies f_{mu} and f_{mv} associated with the peaks of the logarithmic longitudinal and lateral spectra for unstable wind conditions	27
16.	Vertical distributions of the collapsing factors β_u and β_v for unstable wind conditions	28
17.	Dimensionless logarithmic longitudinal and lateral spectra as functions of $0.04 f/f_{mu}$ and $0.033 f/f_{mv}$ for unstable wind conditions	28
18.	Scaled correlation functions for the longitudinal and lateral components of turbulence as functions of the dimensionless space lag ξ for neutral wind conditions	30
19.	Scaled correlation functions for the longitudinal and lateral components of turbulence as functions of the dimensionless space lag ξ for unstable wind conditions	31
20.	Hypothesized scheme of the budget of turbulent energy in the unstable boundary layer for $Ri(18\text{ m}) \approx -0.3$	39

LIST OF SYMBOLS

English Symbols

Symbol	Definition
C	Dimensionless constants that occur in the formulae for the longitudinal and lateral spectra
C_p	Specific heat at constant pressure
E	Kinetic energy per unit mass of the turbulent portion of the flow
f	Dimensionless wave number
f_c	Coriolis parameter
f_m	Dimensionless wave number at which logarithmic spectrum is a maximum
F	Universal function of f and Ri
g	Acceleration of gravity (9.8 m sec^{-2})
H	Vertical heat flux
k_1	Von Karman's constant (0.4)
K_h	Eddy heat conduction coefficient
K_m	Eddy viscosity coefficient
L	Monin and Obukhov stability length
L'	$K_h L / K_m$
L_B	Blackadar's length scale
n	Frequency (Hz)
p'	Pressure fluctuation

LIST OF SYMBOLS (Continued)

Symbol	Definition
r	Dimensionless constants that occur in the formulae for the longitudinal and lateral spectra
Ri	Richardson's number
$R(x)$	Correlation function at space lag x
$S(n)$	Longitudinal or lateral one-dimensional spectrum at frequency n
\bar{T}	Kelvin temperature associated with the mean flow
$\bar{u}(z)$	Mean flow wind speed at height z
u_*	Local friction velocity
u_{*0}	Surface friction velocity
u_{*00}	Surface friction velocity estimated with first estimates of the roughness length
u'	Longitudinal wind speed fluctuation
U	Surface geostrophic wind speed
v'	Lateral wind speed fluctuation
w'	Vertical wind speed fluctuation
x	Longitudinal space lag
z	Height
z_0	Surface roughness length
z_{00}	First estimate of the roughness length

LIST OF SYMBOLS (Concluded)

Symbol	Definition
$()_u$	Quantity associated with longitudinal components of turbulence
$()_v$	Quantity associated with lateral components of turbulence

Greek Symbols

α	Kolomogorov's constant for the one-dimensional longitudinal spectrum (0.146)
β	Vertical collapsing factors
δ	Dimensionless constants that occur in the formulae for the longitudinal and lateral correlation functions
ϵ	The dissipation rate of turbulent kinetic energy
$\bar{\theta}$	Mean flow potential temperature
θ'	Potential temperature fluctuation
κ	Wave number (cycles per meter)
ξ	Dimensionless space lag
ρ	Mean flow density
σ	Standard deviation of the longitudinal or lateral components of turbulence
ϕ	Dimensionless wind shear
ϕ_D	Dimensionless turbulent energy flux divergence
ϕ_ϵ	Dimensionless dissipation rate of turbulent kinetic energy
Ψ	Mean wind speed profile stability defect, a universal function of z/L'

LONGITUDINAL AND LATERAL SPECTRA OF TURBULENCE IN THE ATMOSPHERIC BOUNDARY LAYER

SUMMARY

In many types of space vehicle and aircraft response calculations, engineers employ the Fourier transform to solve the equations of motion which describe and predict the ultimate response of space vehicles to the natural environment. Thus, the input functions which describe the turbulent character of wind loads must be specified in terms of spectra. To develop an engineering boundary layer model of the longitudinal and horizontal lateral spectra of turbulence, a 150-meter meteorological tower was erected at Cape Kennedy, Florida. The tower is instrumented at the 18-, 30-, 60-, 90-, 120-, and 150-meter levels with wind speed and direction sensors which measure the horizontal components of the wind. Temperature sensors are located at the 18-, 30-, 60-, 120-, and 150-meter levels. Fifty one-hour cases of turbulence that occurred during a variety of meteorological conditions were selected for analysis.

Longitudinal (u) and horizontal lateral (v) velocity fluctuation spectra were calculated for each level, resulting in a net total of 300 spectra for each velocity component. It was found that $[nS(n)/u_{*o}^2, f]$ - coordinates, or rather Monin coordinates, fail to produce a vertical collapse of the spectra, where $S(n)$ is the longitudinal or lateral spectral energy density at frequency n (Hz), u_{*o} is the surface friction velocity (calculated with mean wind and temperature profile data), and $f = nz/\bar{u}$, \bar{u} is the mean wind speed at height z . However, it appears that Monin coordinates will collapse spectra with various turbulence intensities at any particular level in the vertical.

To produce a vertical collapse of the spectra, it is assumed, for engineering purposes, that the spectra in Monin coordinates are shape-invariant in the vertical. This hypothesis, which seems to be reasonable, permits a practical approach to developing an engineering spectral model of turbulence. The longitudinal and lateral spectra for the unstable and neutral boundary layers can be represented by the form

$$\frac{nS(n)}{\beta u_*^2} = \frac{\frac{Cf}{f_m}}{\left[1 + 1.5 \left(\frac{f}{f_m} \right)^r \right]^{5/3r}},$$

where C and r are functions of stability. In the neutral boundary layer, β_u and β_v are proportional to $z^{-0.63}$ and $z^{-0.35}$, and in the unstable boundary layer they are proportional to $z^{-0.14}$ and $z^{-0.04}$. The dimensionless wave number f_m associated with the peaks of the logarithmic spectra is an increasing function of z . In neutral air, f_{mu} and f_{mv} are proportional to z and $z^{0.58}$, while in unstable air, they are proportional to $z^{0.87}$ and $z^{0.72}$.

The inverse Fourier transforms (correlation functions) of these spectra are calculated numerically. The integral scale L^* is proportional to z/f_m , so that, in the neutral air, L_u^* is a constant and L_v^* is proportional to $z^{0.42}$, and in unstable air they are proportional to $z^{0.13}$ and $z^{0.28}$.

An analysis of the logarithmic spectrum in the inertial subrange, at the 18-m level, implies that the local mechanical and buoyant production rates of turbulent kinetic energy are balanced by the local dissipation and energy flux divergence, respectively. In addition, the spectral model implies that the dimensionless dissipation rate $k_1 z \epsilon / u_*^3$ is proportional to $z^{0.055}$ and $z^{0.66}$ in the neutral and unstable boundary layers, where k_1 and ϵ denote von Karman's constant and the dissipation rate.

INTRODUCTION

To determine the response of space vehicles, aircraft, tall structures, etc., to atmospheric turbulence, the engineer requires specific information about the spectral nature of atmospheric turbulence. This results because the equations of motion of these vehicles or structures are linear and are solved with Fourier transform techniques and thus the environmental forcing functions must be represented in terms of spectra. Motivated by this requirement, we have developed a model for the longitudinal and horizontal lateral spectra of turbulence for the Kennedy Space Center (KSC). The longitudinal and lateral components of turbulence are the wind fluctuations parallel and normal to the mean wind vector (Fig. 1).

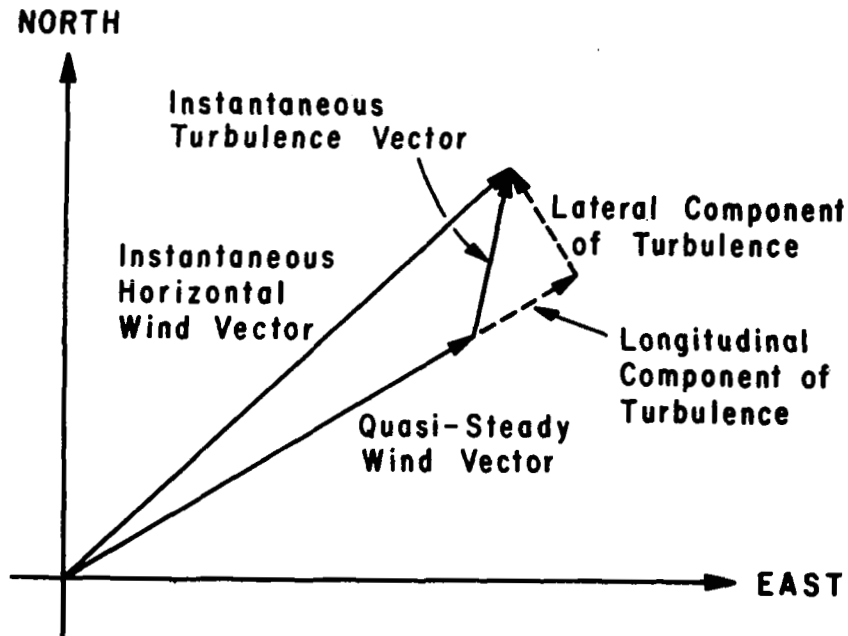


Figure 1. The relationship between the quasi-steady and the instantaneous wind vectors and the longitudinal and lateral components of turbulence.

THE NASA 150-m METEOROLOGICAL TOWER

To obtain micrometeorological data representative of the Cape Kennedy area, especially in the vicinity of the Apollo/Saturn V launch pads, a 150-m meteorological tower was constructed on Merritt Island at KSC. The tower facility, discussed in detail in a report by Kaufman and Keene [1], is only briefly described here.

Terrain Features

Figure 2 shows the location of the facility with respect to the Saturn V space vehicle launch complex 39. The tower, located about five kilometers from the Atlantic Ocean, is situated in a well-exposed area free of near-by structures which could interfere with the air flow.

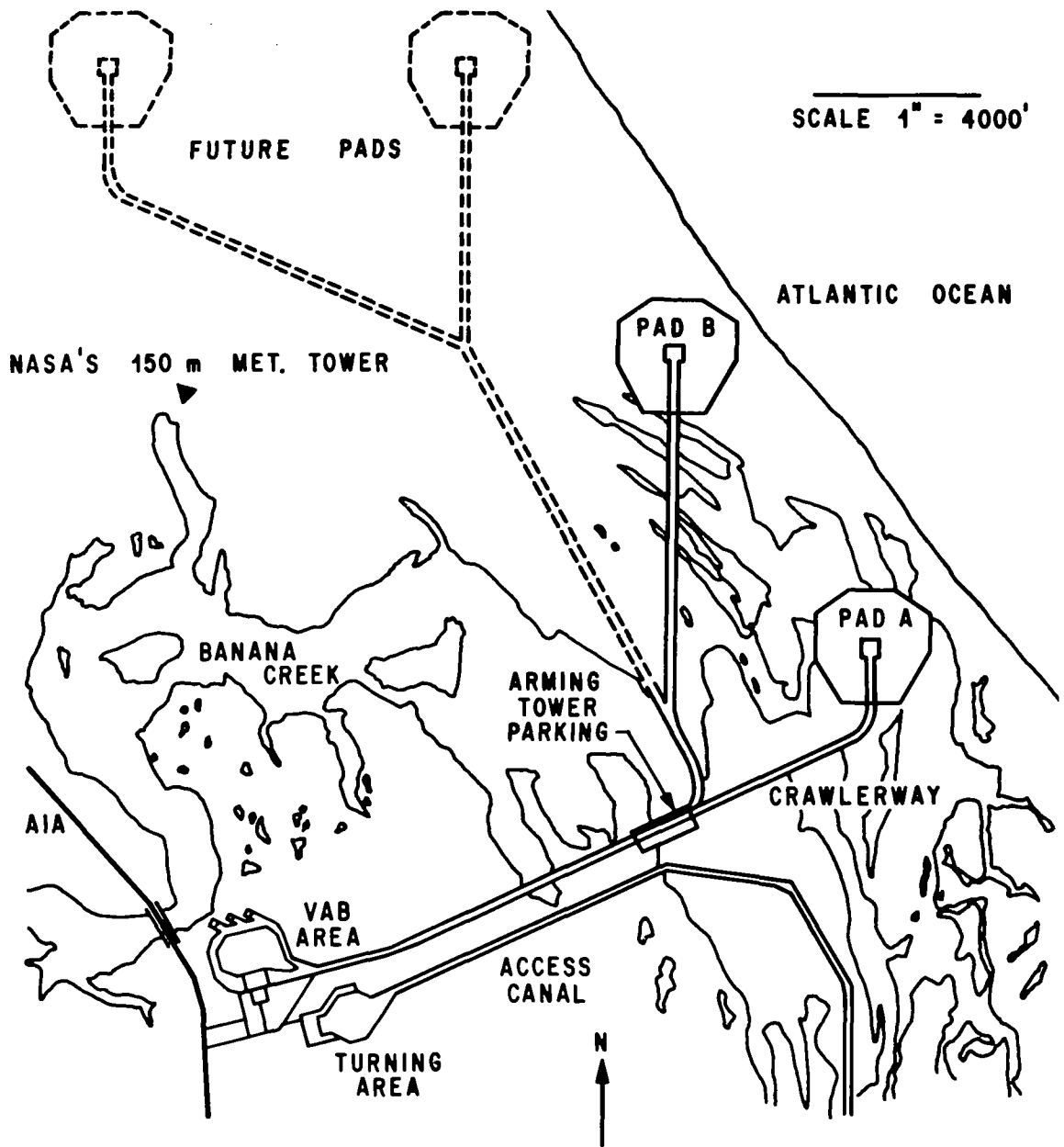


Figure 2. NASA Launch Complex 39, Kennedy Space Center, Florida.

The aerial photograph (Fig. 3) of the terrain surrounding the tower (point T) was taken at 1066 m above mean sea level. In the quadrant from approximately 300 deg north azimuth with respect to the tower, clockwise around to 90 deg, the terrain is homogeneous, being covered with vegetation



Figure 3. Aerial view of the terrain surrounding the NASA 150-m meteorological tower.

about 0.5 to 1.5 m high. Another homogeneous area with the same type of vegetation occurs in the 135- to 160-deg quadrant. The areas A (230-300 deg), B (90-135 deg), and C (160-180 deg) are covered with trees from about 10 to 15 m tall. The distance from the tower to areas A or C is about 200 m, and the distance to area B is about 450 m and the vegetation ranges from one-half to one and one-half meters, as in the area to the north of the tower. To the south-southwest, in the 180- to 230-deg quadrant 225 m from the tower, there is a body of water called Happy Creek.

Instrumentation

The complete tower facility comprises two towers, one 18 m and the other 150 m high (Fig. 4). The levels on both towers are instrumented with

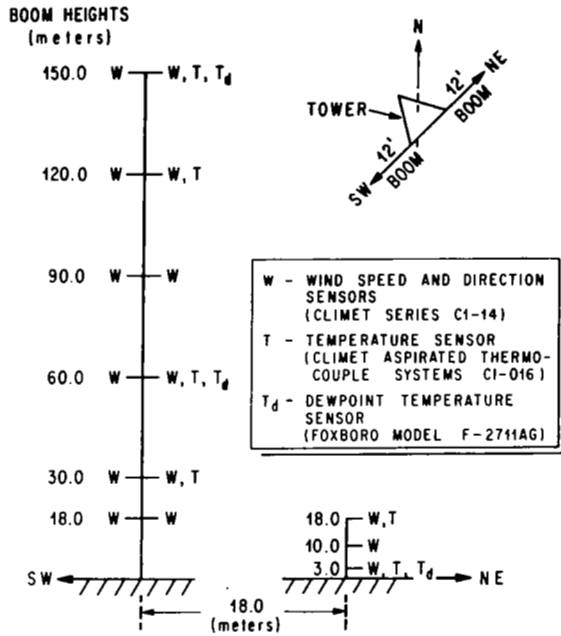


Figure 4. Location of instrumentation on the NASA 150 m meteorological tower at Kennedy Space Center, Florida.

Climet (Model CI-14) wind sensors. Temperature sensors, Climet (Model CI-016) aspirated thermocouples, are located at the 3- and 18-m levels on the small tower and at the 30-, 60-, 120-, and 150-m levels on the large tower. Foxboro (Model F-2711AG) dewpoint temperature sensors are located at the 60- and 150-m levels on the large tower and at the 3-m level on the 18-m tower. Wind speed and direction data can be recorded on both paper strip charts and analog magnetic tapes with an Ampex FR-1200 fourteen-channel magnetic tape recorder which uses a 14-inch reel. The temperature and dewpoint data are recorded on paper strip charts. To avoid tower interference of the flow, the large tower is instrumented with two banks of wind sensors. The details of how and when one switches from one bank of instrumentation to the other is discussed by Kaufman and Keene [1]. During a test in which the wind data are stored on magnetic tape, only one bank

of instrumentation is used, thus avoiding interruption of the wind data signals within any magnetic tape recording period. This continuity of signals prevents data processing difficulties when converting analog tapes to digital tapes.

Surface Roughness Length (z_0)

In an earlier report, Fichtl [2] discussed the surface roughness length configuration associated with the NASA meteorological tower. This analysis was based upon wind profile laws that are consistent with the Monin-Obukhov similarity hypothesis. The calculations of z_0 were based on wind data

obtained at the 18- and 30-m levels and on temperature data obtained at the 18- and 60-m levels. Most of the measurements were obtained during the hours of 0700 and 1600 EST, and the gradient Richardson numbers at 23 m (geometric mean height between 18 and 30 m) for the 39 cases ranged between -5.82 and +0.079. The results of these calculations, shown in Figure 5, show the effect the terrain features have upon the surface roughness. Later, an analysis of the energy budget at 18 m will show that these roughness lengths are too large.

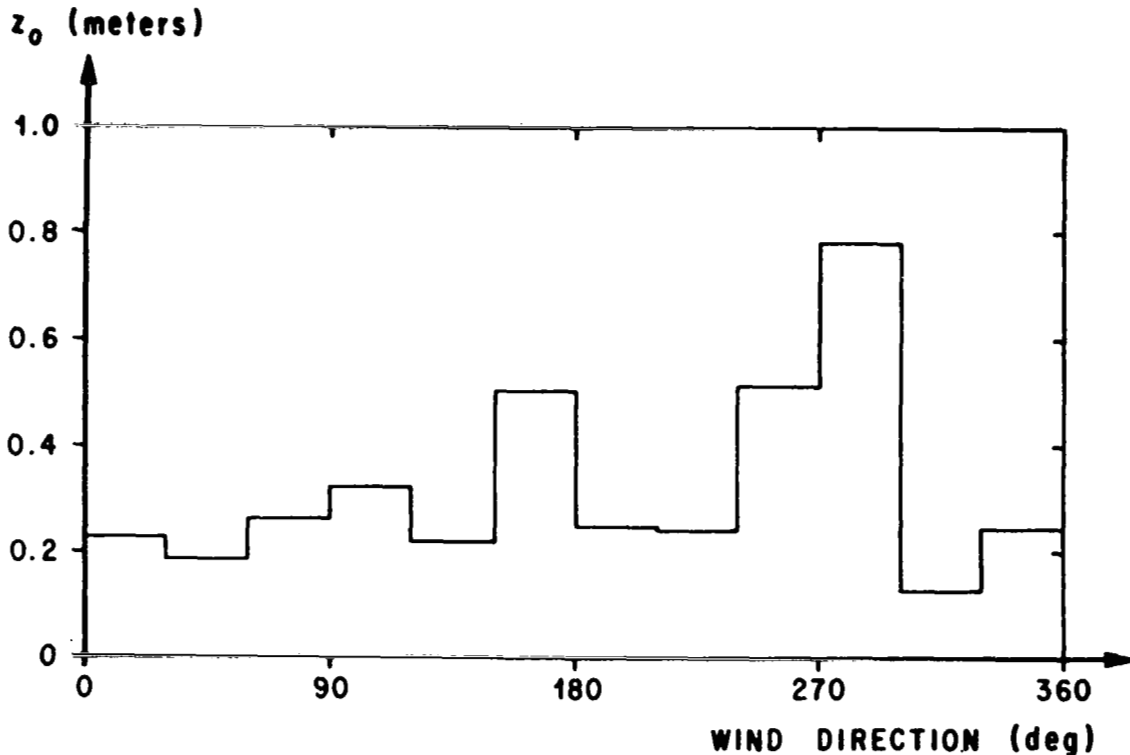


Figure 5. Tentative azimuthal distribution of the surface roughness length at the NASA 150-m meteorological tower site.

COMPUTATIONS AND INITIAL SCALING

To establish a spectral model of turbulence for the Kennedy Space Center, approximately 50 cases of turbulence were analyzed. The procedure used to calculate the longitudinal and lateral components of turbulence

consisted of (1) converting the digitized wind speeds and directions (10 data points per second) into the associated north-south and east-west components and averaging these components over the duration time of each test, (2) calculating the mean wind speed and direction with the averaged components, (3) projecting the original digitized data onto the mean wind vector and subtracting the mean wind speed to yield the longitudinal components of turbulence, and (4) projecting the original digitized data onto a normal-to-the-mean wind vector to obtain the lateral components of turbulence. Trends contained within the data were removed by fitting the longitudinal and lateral components of turbulence to second order polynomials and, in turn, subtracting these polynomials from the component time histories. To reduce computation time, the data, with trend removed, were block-averaged over half-second intervals. The longitudinal and lateral spectra were calculated by using the standard correlation Fourier transform methods given by Blackman and Tukey [3]. These spectra were corrected for the half-second block-averaging operation with the procedure given by Pasquill [4] and for the response properties of the instrumentation.

To combine the spectra for each level on the tower, it was assumed that the similarity theory of Monin [5] for the vertical velocity spectrum could be applied to the longitudinal and lateral spectra, so that

$$\frac{nS(n)}{u_{*0}^2} = F(f, Ri) \quad , \quad (1)$$

where $nS(n)$ is the logarithmic longitudinal or lateral spectrum associated with frequency n (Hz), and u_{*0} is the surface friction velocity, or rather, the square root of the tangential eddy stress per unit mass. F is tentatively a universal function of the dimensionless wave number f and the gradient Richardson number Ri . The dimensionless wave number is given by

$$f = \frac{nz}{\bar{u}(z)} \quad . \quad (2)$$

Because the tower did not have the capability to measure vertical velocity fluctuations, the Reynolds stress, and hence u_{*0}^2 , cannot be calculated with first principles; viz, $u_{*0}^2 = \overline{-u'w'}$, where u' and w' are the longitudinal

and vertical velocity fluctuations and the overbar denotes a time-averaging operator. However, an estimate of the surface friction velocity can be calculated from mean wind and temperature profile data.

According to Lumley and Panofsky [6], the mean wind profile in approximately the first 30 m of the atmosphere is given by

$$\bar{u}(z) = \frac{u_{*o}}{k_1} \left[\ln \frac{z}{z_o} - \Psi \left(\frac{z}{L'} \right) \right] , \quad (3)$$

where k_1 is von Karman's constant with numerical value approximately equal to 0.4, and Ψ is a universal function of z/L' . L' is a stability length given by

$$L' = \frac{u_{*o} \frac{d\bar{u}}{dz} \bar{T}}{k_1 g \frac{d\bar{\theta}}{dz}} , \quad (4)$$

where \bar{T} and $\bar{\theta}$ are the Kelvin and potential temperatures associated with the mean flow. The quantity z/L' is related to the gradient Richardson number

$$Ri = \frac{\frac{g}{\bar{\theta}} \frac{d\bar{\theta}}{dz}}{\left(\frac{d\bar{u}}{dz} \right)^2} \quad (5)$$

through the relationships

$$\frac{z}{L'} = \frac{Ri}{(1 - 18 Ri)^{1/4}} \quad (Ri < -0.01) , \quad (6)$$

$$\frac{z}{L'} = Ri \quad (-0.01 \leq Ri \leq 0.01) , \quad (7)$$

and

$$\frac{z}{L'} = \frac{Ri}{1 - 7 Ri} \quad (0.1 \geq Ri > 0.01) \quad . \quad (8)$$

Equation (6) is a form of the KEYPS [6] equation. The function $\Psi(z/L')$ associated with equations (7) and (8) are given by

$$\Psi\left(\frac{z}{L'}\right) = -4.5 \frac{z}{L'} \quad (-0.01 \leq Ri \leq 0.01) \quad (9)$$

and

$$\Psi\left(\frac{z}{L'}\right) = -7 \frac{z}{L'} \quad (0.1 \geq Ri > 0.01) \quad . \quad (10)$$

Lumley and Panofsky [6] have graphically indicated the function $\Psi(z/L')$ for $Ri < -0.01$ and the function

$$\Psi\left(\frac{z}{L'}\right) = 0.044 \left(\frac{-\frac{z}{L'}}{0.01}\right)^{1.0674 - 0.678 \ln\left(\frac{-\frac{z}{L'}}{0.01}\right)} \quad (Ri < -0.01) \quad (11)$$

faithfully reproduces their curve.

The calculation of u_{*0} was based upon the wind data measured at the 18- and 30-m levels and the temperature data measured at the 18- and 60-m levels. Temperatures at the 30-m level were estimated by logarithmically interpolating between the 18- and 60-m levels. An estimate of the gradient Richardson number, equation (5), at the 23-m level (geometric mean height between the 18- and 30-m levels) was determined by assuming that the mean wind speed and temperature are logarithmically distributed between these levels. The gradient Richardson number estimated in this manner is given by

$$\text{Ri}(z_g) = \frac{g}{\overline{T}(z_g)} \left[\frac{\overline{T}(z_2) - \overline{T}(z_1)}{z_g \ln \frac{z_2}{z_1}} + \frac{g}{C_p} \right] \left[\frac{\overline{u}(z_2) - \overline{u}(z_1)}{z_g \ln \frac{z_2}{z_1}} \right]^{-2}, \quad (12)$$

where $\overline{T}(z)$ is the mean temperature at height z , z_1 , and z_2 , denotes 18 and 30 m, $z_g = \sqrt{z_1 z_2}$.

To calculate u_{*0} , z_g/L' was evaluated for each case by means of one of the three equations, (6) through (8), corresponding to the appropriate Richardson number class. L' was then assumed to be invariant with height, and $\Psi(18/L')$ was estimated with equations (9) through (11). Equation (3) was then evaluated at the 18-m level and solved to yield u_{*0} . The values of z_0 used for this calculation are given in Figure 5.

THE INERTIAL SUBRANGE AND REVISED VALUES OF THE SURFACE ROUGHNESS LENGTHS

In the inertial subrange, the longitudinal spectrum is given by

$$\frac{nS_u(n)}{u_{*0}^2} = \alpha k_1^{-2/3} \phi_\epsilon^{2/3} f^{-2/3}, \quad (13)$$

where α is Kolmogorov's constant with a numerical value equal to 0.146 according to Record and Cramer [7]. The quantity ϕ_ϵ is the dimensionless dissipation rate of turbulent kinetic energy per unit mass given by

$$\phi_\epsilon = \frac{k_1 z \epsilon}{u_{*0}^3}, \quad (14)$$

where ϵ is the rate of dissipation of turbulent energy. Below 30 m, where the Monin and Obukhov similarity hypothesis for the wind profile is expected to be valid, ϕ_ϵ is a function of Ri only.

Inferences concerning the dependence of ϕ_ϵ on Ri can be made with the aid of the eddy energy equation. For homogeneous terrain, this equation is given by

$$\frac{d\bar{E}}{dt} = u_*^2 \frac{d\bar{u}}{dz} + \frac{H}{C_p \rho} \frac{g}{T} - \epsilon - \frac{d}{dz} \left(\frac{\overline{p'w'}}{\rho} + \overline{w'E} \right) , \quad (15)$$

where $\frac{H}{C_p \rho}$ is the eddy heat flux $\overline{\theta'w'}$, ρ is the mean density, E the turbulent kinetic energy per unit mass, p' and w' denote the turbulent fluctuations of pressure and vertical velocity, and u_* is the local friction velocity ($u_* = u_{*0}$ in the Monin layer). Following Busch and Panofsky [8], we write equation (15) in dimensionless form, so that

$$\frac{k_1 z}{u_{*0}^3} \frac{d\bar{E}}{dt} = \left(\frac{u_*}{u_{*0}} \right)^2 \phi - \frac{z}{L} - \phi_\epsilon - \phi_D . \quad (16)$$

The terms in this expression are in one-to-one correspondence with those of equation (15); however, the pressure term has been neglected. L is the Monin-Obukhov stability length where

$$L = - \frac{u_{*0}^3 C_p \rho \bar{T}}{k_1 g H} . \quad (17)$$

Near the ground a majority of meteorological conditions are characterized, at least approximately, by horizontal homogeneity, steady mean wind with no change of wind direction with height, and steady heating from below. In most cases, it is reasonable to make these assumptions with regard to the KSC tower site. Thus, to a reasonable degree of approximation, we have $\overline{dE}/dt = 0$, and equation (16) implies that in the Monin layer

$$\phi - \frac{z}{L} - \phi_\epsilon - \phi_D = 0 . \quad (18)$$

Various authors have hypothesized schemes to balance the left-hand side of equation (18). Lumley and Panofsky [6] suggest that the local mechanical energy production is balanced by the local viscous dissipation, so that

$$\phi_{\epsilon} = \phi \quad , \quad (19)$$

and thus, the buoyant energy production is balanced by the energy flux divergence term, making

$$\phi_D = -\frac{z}{L} \quad . \quad (20)$$

Busch and Panofsky [8] suggest the flux divergence term is negligible and the local viscous dissipation is balanced by both the local mechanical and buoyant energy productions, so that

$$\phi_{\epsilon} = \phi - \frac{z}{L} \quad . \quad (21)$$

We shall call equations (19) and (21) hypotheses I and II.

According to Lumley and Panofsky,

$$\phi = (1 - 18 Ri)^{-1/4} \quad (22)$$

in the unstable Monin layer. This form of the dimensionless shear is consistent with equation (6). Upon combining equations (13), (19), and (22), the spectrum in the Kolmogorov subrange for hypothesis I takes the form

$$\left[\frac{n S_u(n)}{u_*^2} \right]_I = \alpha k_1^{-2/3} (1 - 18 Ri)^{-1/6} f^{-2/3} \quad . \quad (23)$$

Combination of equations (6), (13), (17), (21), and (22) yields

$$\left[\frac{n S_u(n)}{u_{*o}^2} \right]_{II} = \alpha k_1^{-2/3} \left[\frac{1 - Ri \frac{K_m}{K_h}}{(1 - 18 Ri)^{1/4}} \right]^{2/3} f^{-2/3} \quad (24)$$

for hypothesis II, where K_m and K_h are the eddy viscosity and heat conduction coefficients given by

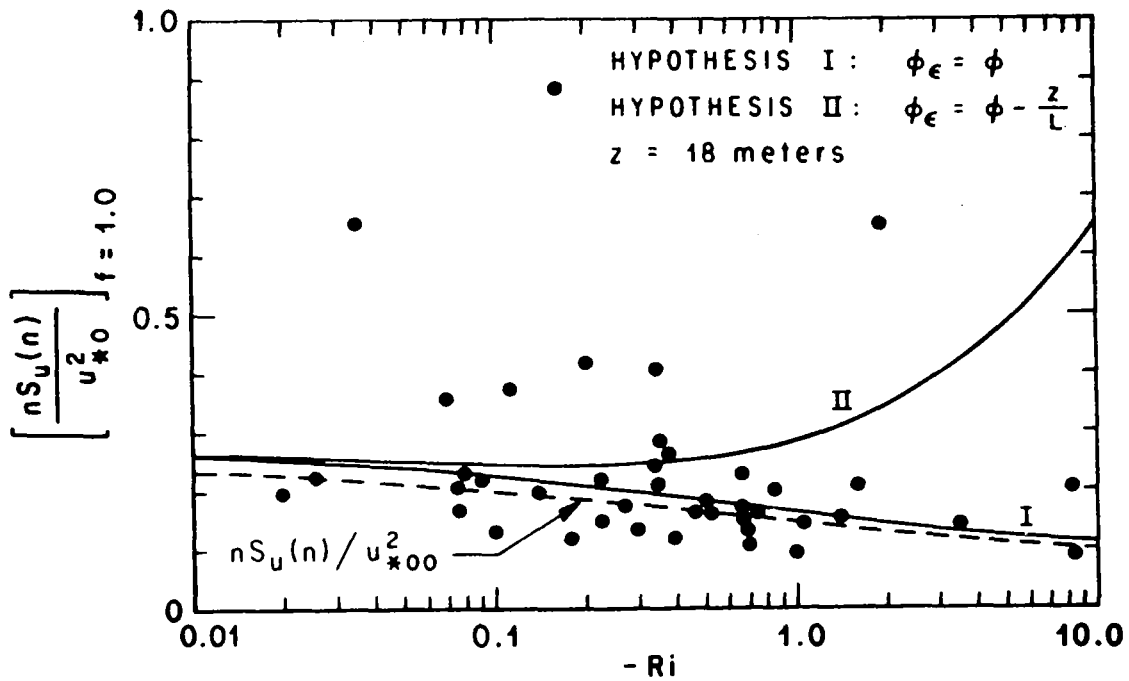
$$K_m = \frac{u_*^2}{\frac{d\bar{u}}{dz}} \quad (25)$$

and

$$K_h = - \frac{H}{C_p \rho \frac{d\bar{\theta}}{dz}} \quad (26)$$

Figure 6 illustrates $\left[n S_u(n) / u_{*o}^2 \right]_I$ and $\left[n S_u(n) / u_{*o}^2 \right]_{II}$ as functions of $-Ri$ for $f = 1.0$ and $K_h / K_m = 1.3$. As $-Ri$ approaches infinity, $\left[n S_u(n) / u_{*o}^2 \right]_I$ converges to zero, and $\left[n S_u(n) / u_{*o}^2 \right]_{II}$ diverges. As $-Ri$ approaches zero, $\left[n S_u(n) / u_{*o}^2 \right]_I$ asymptotically approaches $\left[n S_u(n) / u_{*o}^2 \right]_{II}$. The difference between $\left[S_u \right]_I$ and $\left[S_u \right]_{II}$ is small (within the noise level of the data) for $Ri > -1.0$, and thus it is difficult to reject one hypothesis in favor of the other for sufficiently small $-Ri$.

At the 18-m level, longitudinal spectra were used to test hypotheses I and II, and the cut-off value of f was approximately 2.0 in most of the cases. Actually, the Kolmogorov subrange occurs at much greater dimensionless wave numbers; however, the $-5/3$ power law behavior extends down to values of f on the order of unity for the longitudinal spectrum, while this is not true



Note: The variations of $\left[\frac{nS_u(n)}{u_{*0}^2} \right]_{f=1.0}$ for hypotheses I and II are indicated. The dashed curve corresponds to $\left[\frac{nS_u(n)}{u_{*00}^2} \right]_{f=1.0}$ with $z_0 = 0.18$ m and $z_{00} = 0.23$ m for a type I energy budget.

Figure 6. The dimensionless logarithmic longitudinal spectrum at $f = 1.0$ and $z = 18$ m as a function of $-Ri$.

for the lateral spectrum. In addition, the Monin and Obukhov similarity hypothesis for the wind profile upon which the calculation of u_{*0} is based is, at most, valid below 30 meters. Accordingly, the 18-m longitudinal spectra are the only ones that could be used to test the validity of hypotheses I and II without introducing assumptions about how the eddy stress and heat flux vary with height.

In Figure 6 we have plotted the experimental values of $nS_u(n)/u_{*0}^2$ for the longitudinal spectrum for $f = 1.0$ as a function of $-Ri$. The experimental results scatter about the dashed line, but they appear to favor hypothesis I more than hypothesis II, especially for $Ri \leq -3.0$. If we accept hypothesis I, then we must conclude that the scaling velocities, u_{*0} are too large and thus the roughness lengths are too large. If we reject hypothesis I, then we must accept a more complicated energy balance system. We shall invoke Ockham's razor, accept hypothesis I, and correct the surface roughness lengths.

We denote the surface roughness lengths in Figure 5 with z_{oo} , and the correct ones resulting from the analysis of the longitudinal spectrum will be denoted with z_o . The corresponding friction velocities will be denoted by u_{*oo} and u_{*o} , respectively. The longitudinal spectrum in the inertial subrange, scaled in terms of u_{*oo} , is given by

$$\frac{nS_u(n)}{u_{*oo}^2} = \left(\frac{\ln \frac{z}{z_{oo}} - \Psi(Ri)}{\ln \frac{z}{z_o} - \Psi(Ri)} \right)^2 \propto k_1^{-2/3} (1 - 18 Ri)^{-1/6} f^{-2/3} \quad (27)$$

The data points in Figure 6 correspond to $nS_u(n)/u_{*oo}^2$, not $nS_u(n)/u_{*o}^2$. At neutral stability ($Ri = 0$), we have $\Psi(0) = 0$, and equation (27) reduces to

$$\left(\frac{\ln \frac{z}{z_{oo}}}{\ln \frac{z}{z_o}} \right)^2 = \frac{nS_u(n) k_1^{2/3}}{u_{*oo}^2 \alpha} \quad (28)$$

for $f = 1.0$. Denoting the right-hand side of equation (28) by χ^{-2} and solving for z_o , we find

$$z_o = z^{1-\chi} z_{oo}^\chi \quad (29)$$

Upon extrapolating the data in Figure 6 to $Ri = 0$ at $f = 1$, we find $nS_u(n)/u_{*00}^2 = 0.24$, so that $\chi = 1.059$. The new values of z_0 for this value of χ and $z = 18$ m are shown in Figure 7. Substitution of equation (29) into equation (27) yields

$$\frac{nS_u(n)}{u_{*00}^2} = \left[\frac{\chi^{-1} \ln \frac{z}{z_0} - \Psi(Ri)}{\ln \frac{z}{z_0} - \Psi(Ri)} \right]^2 \propto k_1^{-2/3} (1 - 18 Ri)^{-1/6} f^{-2/3} \quad (30)$$

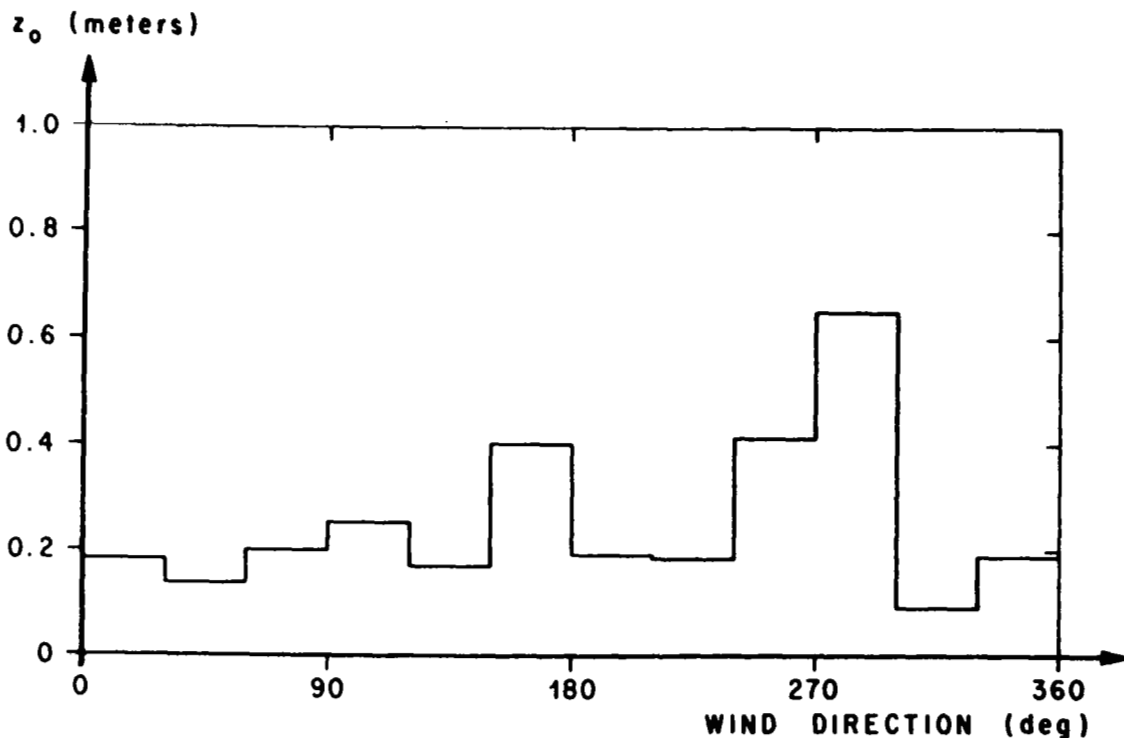


Figure 7. Revised azimuthal distribution of the surface roughness length based upon energy budget considerations at $z = 18$ m.

The dashed curve in Figure 6 represents $nS_u(n)/u_{*00}^2$ as a function of Ri according to equation (30) for $\chi = 1.059$ and $z_0 = 0.18$ m ($z_{00} = 0.23$ m), and it seems to fit the data reasonably well. The function $nS_u(n)/u_{*00}^2$ for the range of variation of z_0 illustrated in Figure 7 departs from the dashed

curve by only a few tenths of one percent. This means a spectral model of the longitudinal and lateral components of turbulence can be developed in terms of u_{*00} , and the final results can be corrected by applying a multiplicative factor which is a function of the Richardson number and a typical roughness length for the site.

EXTRAPOLATION TO NEUTRAL WIND CONDITIONS ($Ri = 0$)

The meteorological conditions of particular engineering interest are those associated with mean wind speeds at the 18-m level which are greater than approximately 10 m sec^{-1} . During these flow conditions, the boundary layer is well mixed so that vertical gradients of the mean flow entropy and thus potential temperature are small and the wind shears are large. Thus, the Richardson number vanishes or at least becomes very small. Accordingly, the neutral longitudinal and lateral spectra are of particular interest in the design and operation of space vehicles. The neutral spectra were determined by extrapolating the data to $Ri = 0$ by the procedure developed by Berman [9]. Scaled spectra $nS(n)/u_{*00}^2$ were plotted against Ri for various values of f , and smooth curves were drawn by eye. Of course, the data points scattered about this line. The values of $nS(n)/u_{*00}^2$ at $Ri = 0$ were then read off and corrected by multiplying the results by χ^2 to yield the neutral spectra $nS(n)/u_{*0}^2$ for the various levels on the tower. The results of this graphical process are shown in Figures 8 and 9, where the positions of the maxima shift toward higher values of f as the height increases. This means that Monin coordinates $[nS(n)/u_{*0}^2, f]$ fail to collapse the spectra in the vertical so that $F(f, Ri)$ is not a universal function, and thus an added height dependence should be included in the analysis. Busch and Panofsky [8] have obtained similar results from analyses of tower data from Round Hill. The failure of the Monin coordinates to collapse the spectra in the vertical can be attributed to vertical variations in both the Reynolds stress and the length scale used to scale the wave number $n/\bar{u}(z)$.

Above the Monin layer ($z < 30 \text{ m}$) in the Ekman layer ($z > 30 \text{ m}$), the tangential Reynolds stress decreases with height. In addition, the variances of the longitudinal and lateral components of turbulence are decreasing functions of z . Thus, if u_* is the correct scaling velocity, scaling the spectra with

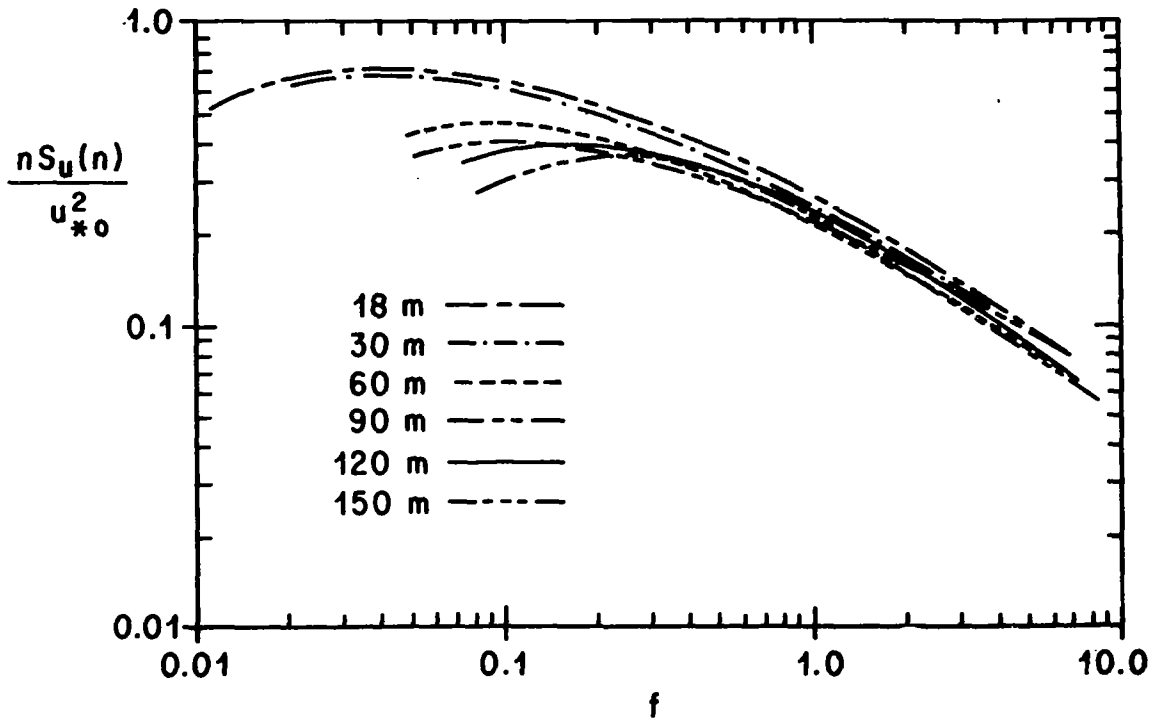


Figure 8. Dimensionless logarithmic longitudinal spectra for neutral wind conditions.

the surface value of the friction velocity will cause the scaled spectra at the upper levels to fall below the 18-m spectra.

By scaling the wave number with z , we have assumed that the integral scales of the longitudinal and lateral components of turbulence are proportional to z . One might suspect from the behavior of eddy coefficients [10] that, if the local integral scales have vertical variations, they should increase at a rate slower than z . In addition, we have no knowledge that the integral scales of the longitudinal and lateral spectra should have the same vertical variation. However, the analysis showed that Monin coordinates will collapse spectra with various turbulence intensities at any particular level in the vertical.

To produce a vertical collapse of the data, it was assumed, for engineering purposes, that the spectra in Monin coordinates are shape-invariant in the vertical. This hypothesis seems to be reasonable and permits a practical approach to developing an engineering spectral model of turbulence.

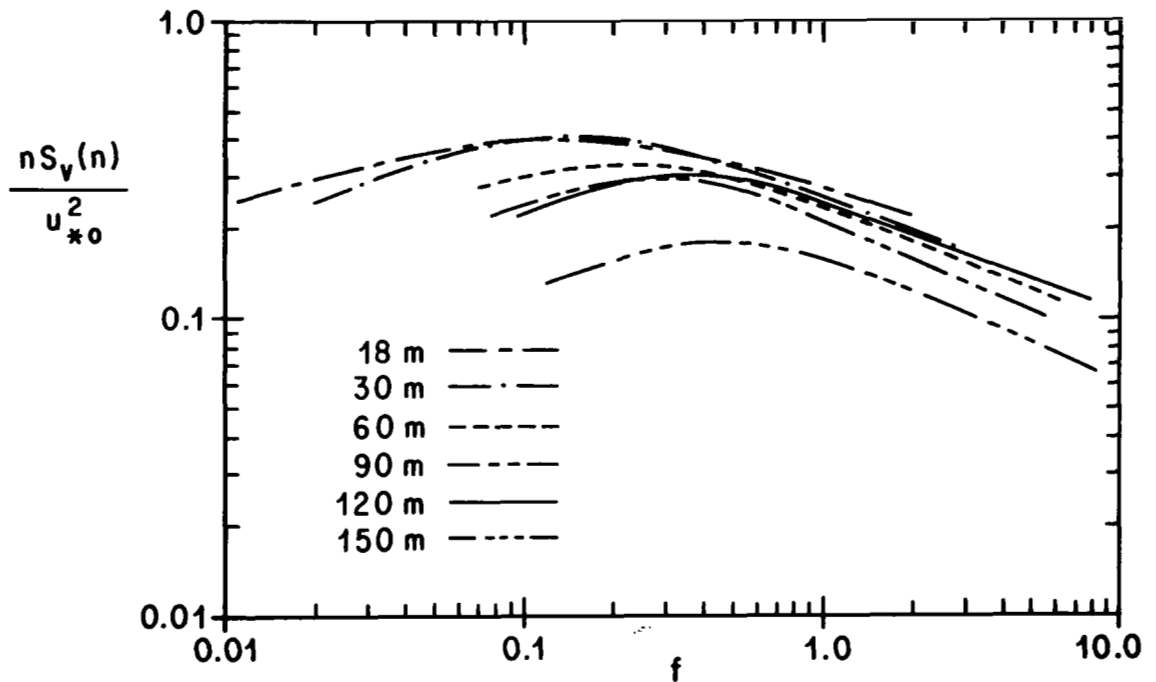


Figure 9. Dimensionless logarithmic lateral spectra for neutral wind conditions.

The Longitudinal Spectrum

The vertical variation of the dimensionless wave number f_{mu} associated with the peak of the logarithmic spectrum scaled in Monin coordinates is given in Figure 10. A least-squares analysis of the data in this figure yielded the result

$$f_{\text{mu}} = 0.03 \left(\frac{z}{18} \right) \quad , \quad (31)$$

where z is in meters. A plot of $nS_u(n)/u_*0^2$ versus f/f_{mu} will shift the spectra at the various levels, so that all the peaks of the logarithmic longitudinal spectra are located at $f/f_{\text{mu}} = 1$. Values of f_{mu} from other tower sites are indicated in Figure 10.

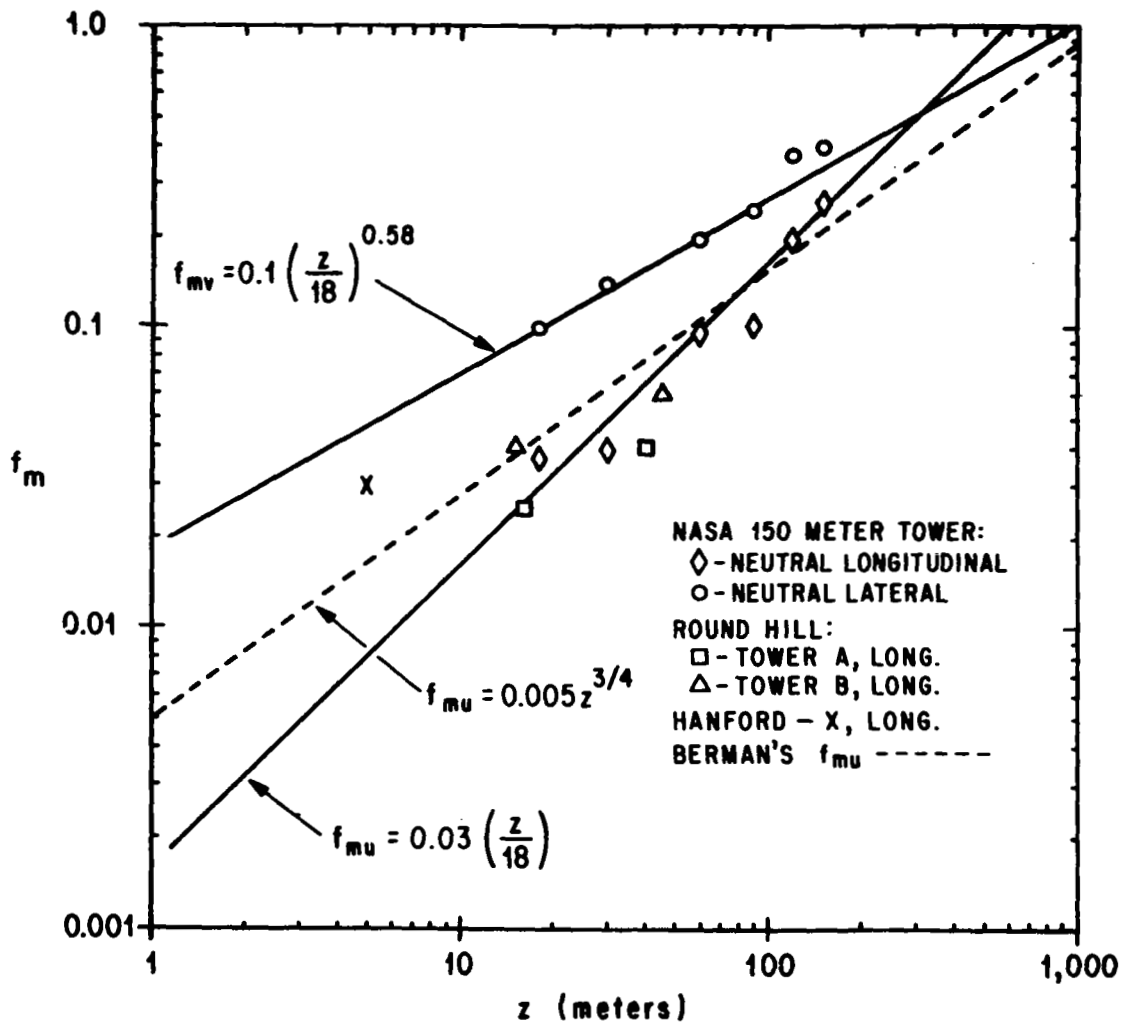


Figure 10. Vertical distributions of the dimensionless frequencies f_{mu} and f_{mv} associated with the peaks of the logarithmic longitudinal and lateral spectra for neutral stability conditions.

The average ratio β_u of the shifted spectrum at level z and the 18-m spectrum, $\left[\frac{S_u(f/f_{mu}, z)}{S_u(f/f_m, 18)} \right]$, is shown in Figure 11. A least-squares analysis of these data yielded the result

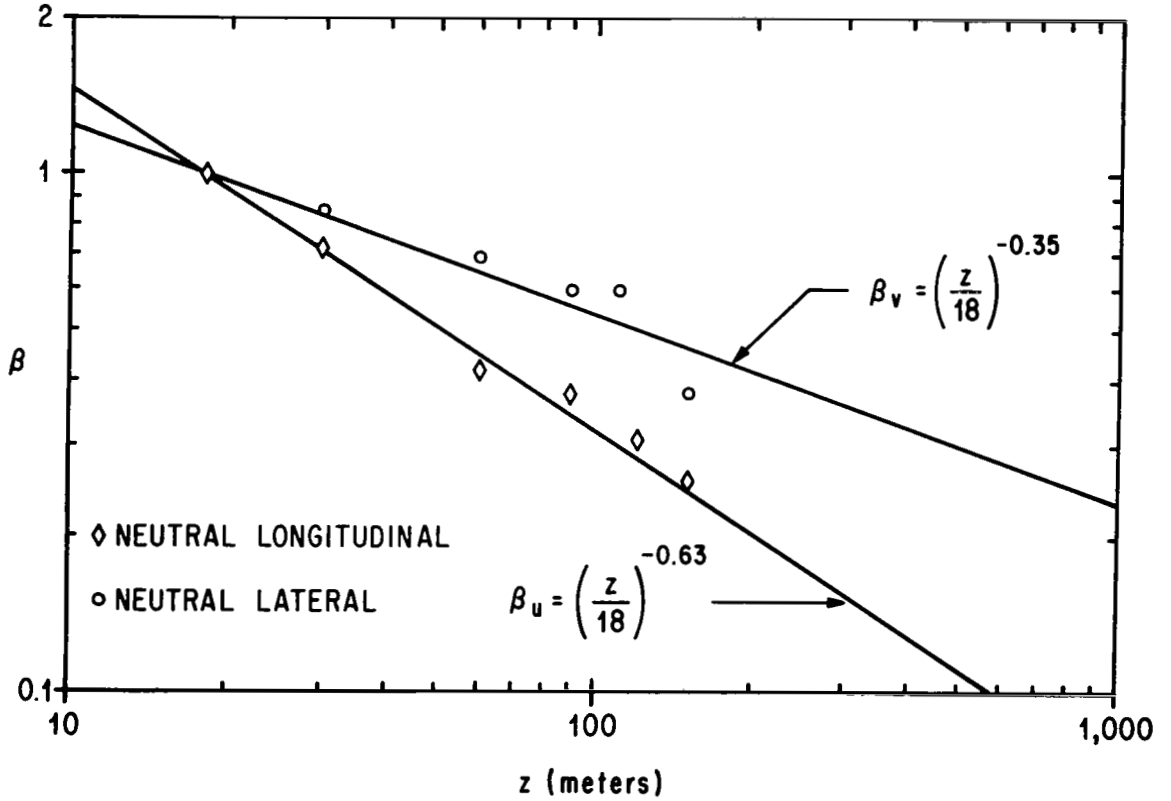


Figure 11. Vertical distributions of the collapsing factors β_u and β_v for neutral stability conditions.

$$\beta_u = \left(\frac{z}{18} \right)^{-0.63}, \quad (32)$$

where z is in meters. A plot of $nS_u(n)/\beta_u u_{*o}^2$ versus f/f_{mu} will collapse the longitudinal spectra. The collapsed longitudinal data are plotted as a function of $0.03 f/f_{mu}$ in Figure 12.

The function

$$\frac{nS_u(n)}{\beta_u u_{*o}^2} = \frac{C_u \frac{f}{f_{mu}}}{\left[1 + 1.5 \left(\frac{f}{f_{mu}} \right)^{r_u} \right]^{5/3r_u}} \quad (33)$$

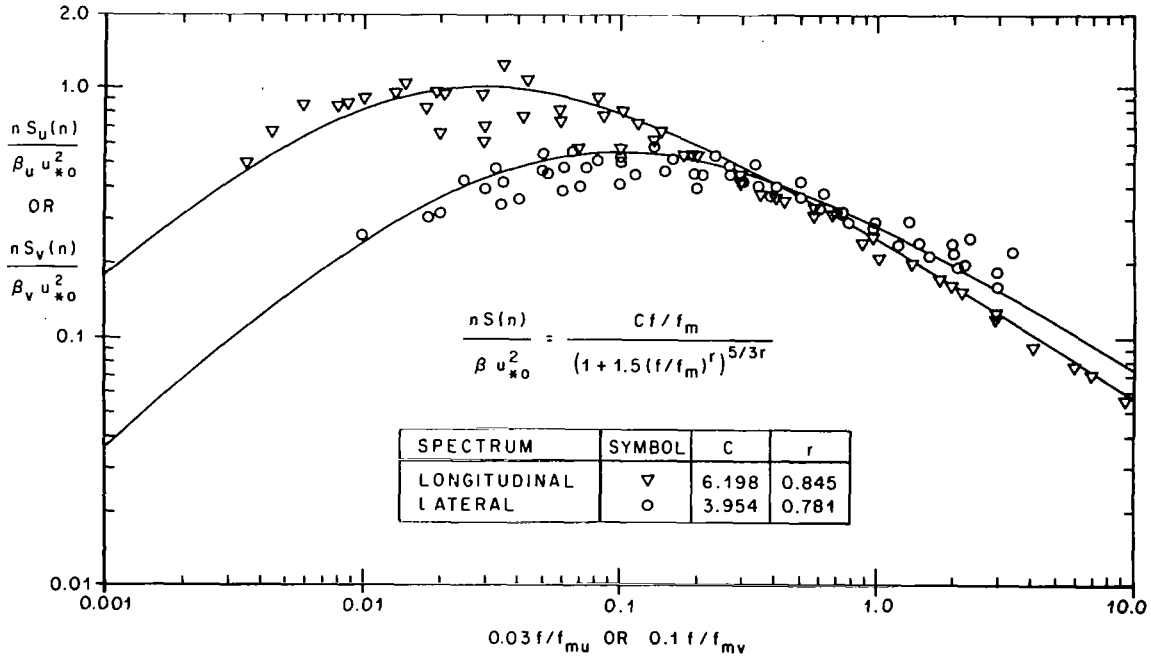


Figure 12. Dimensionless logarithmic longitudinal and lateral spectra as functions of $0.03 f/f_{\mu}$ and $0.1 f/f_{\nu}$ for neutral stability conditions.

was selected to represent the longitudinal spectrum, where C_u and r_u are positive constants, determined by a least-squares analysis. For sufficiently small values of f , $nS_u(n)/\beta_u u_{*o}^2$ asymptotically behaves like f/f_{μ} . This behavior is correct for a one-dimensional spectrum. At large values of f , $nS_u(n)/\beta_u u_{*o}^2$ asymptotically behaves like $(f/f_{\mu})^{-2/3}$, consistent with the concept of the inertial subrange. The maximum value of equation (33) occurs at $f = f_{\mu}$. Various authors have suggested formulae like equation (33) to represent the longitudinal spectrum. However, most of the representations have only one adjustable parameter available, while equation (33) has two: C_u and r_u . In this light equation (33) seems to be superior. C_u controls the magnitude of the peak, r_u controls the peakedness, and f_{μ} determines the position of the peak of $nS_u(n)/\beta_u u_{*o}^2$. Upon setting $r_u = 5/3$, we obtain the form of the longitudinal spectrum suggested by Panofsky [6] to

represent the strong wind spectra of Davenport [11]. Von Karman's longitudinal spectrum [12] can be obtained by setting $r_u = 2$. A least-squares analysis of the longitudinal data in Figure 12 revealed that $C_u = 6.198$ and $r_u = 0.845$.

The Lateral Spectrum

The lateral spectra S_v can be collapsed with a procedure like the one used for the longitudinal spectra. However, to determine an analytical expression for the lateral spectrum, special attention must be paid to the inertial subrange to guarantee that $S_u/S_v = 3/4$ [13]. This requirement can be derived from the mass continuity equation for incompressible flow subject to the condition that the eddies are isotropic in the inertial subrange. The experimental values of f_{mv} and β_v are given in Figures 10 and 11. These data show that f_{mv} and β_v can be represented as power laws as for the longitudinal spectra. The function

$$\frac{nS_v(n)}{\beta_v u_*^2} = \frac{C_v \frac{f}{f_{mv}}}{\left[1 + 1.5 \left(\frac{f}{f_{mv}} \right)^{r_v} \right]^{5/3 r_v}} \quad (34)$$

was used to represent the scaled spectra, where C_v and r_v are positive constants. This function behaves like the one chosen for the longitudinal spectrum.

For sufficiently large values of f , the asymptotic behavior of the ratio between equations (33) and (34) is given by

$$\frac{S_u}{S_v} \sim \frac{C_u}{C_v} \frac{\beta_u}{\beta_v} \left(\frac{f_{mu}}{f_{mv}} \right)^{2/3} \left(\frac{3}{2} \right)^{5/3} \left(\frac{1}{r_v} - \frac{1}{r_u} \right) \quad (35)$$

In the inertial subrange we must have $S_u/S_v = 3/4$, so that upon substituting this ratio into equation (35), we obtain a relationship that can be used as a constraint in the determination of values of C_v and r_v and functions to represent β_v and f_{mv} . The values $C_v = 3.954$ and $r_v = 0.781$, and the functions

$$f_{mv} = 0.1 \left(\frac{z}{18} \right)^{0.58} \quad (36)$$

and

$$\beta_v = \left(\frac{z}{18} \right)^{-0.35} \quad (37)$$

along with the longitudinal parameters, will satisfy the conditions of equation (35) and simultaneously give a good fit to the data (z is in meters). The collapsed lateral spectra and the functions given by equations (33) and (34) are shown in Figure 12.

UNSTABLE SPECTRA

To develop an engineering model for unstable conditions, the unstable spectra were averaged and then corrected by multiplication with

$$\left[\frac{\ln \frac{z}{z_0} - \Psi(Ri)}{\chi^{-1} \ln \frac{z}{z_0} - \Psi(Ri)} \right]^2$$

for $z = 18$ m, $z_0 = 0.18$ m, and $Ri = -0.3$. The longitudinal and lateral spectra for the mean unstable conditions are shown in Figures 13 and 14. The unstable spectra were collapsed by using the procedures for the neutral boundary layer, and the functions given by equations (33) and (34) appear to be

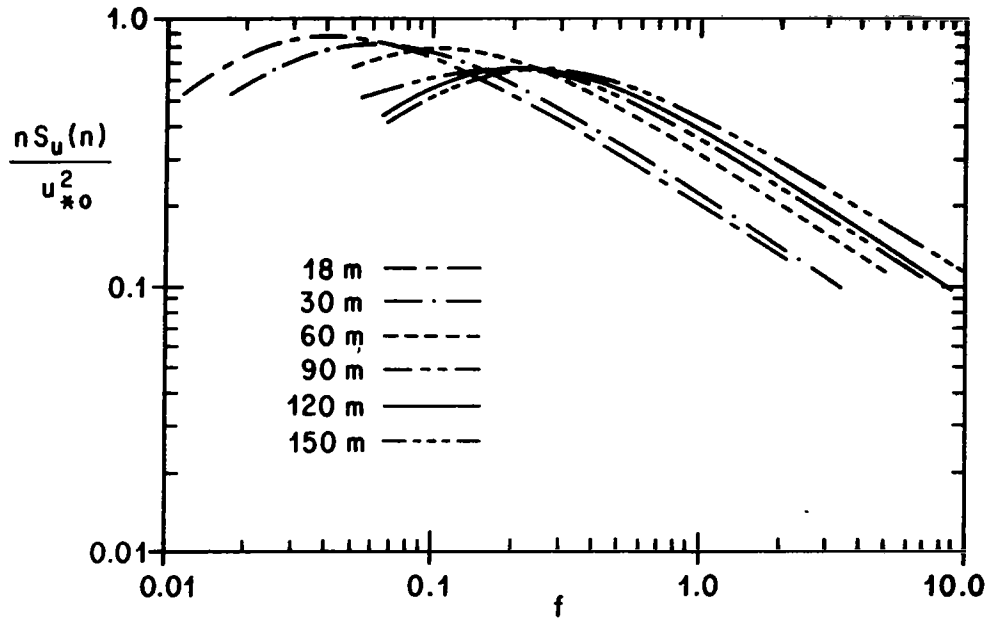


Figure 13. Dimensionless logarithmic longitudinal spectra for unstable wind conditions.

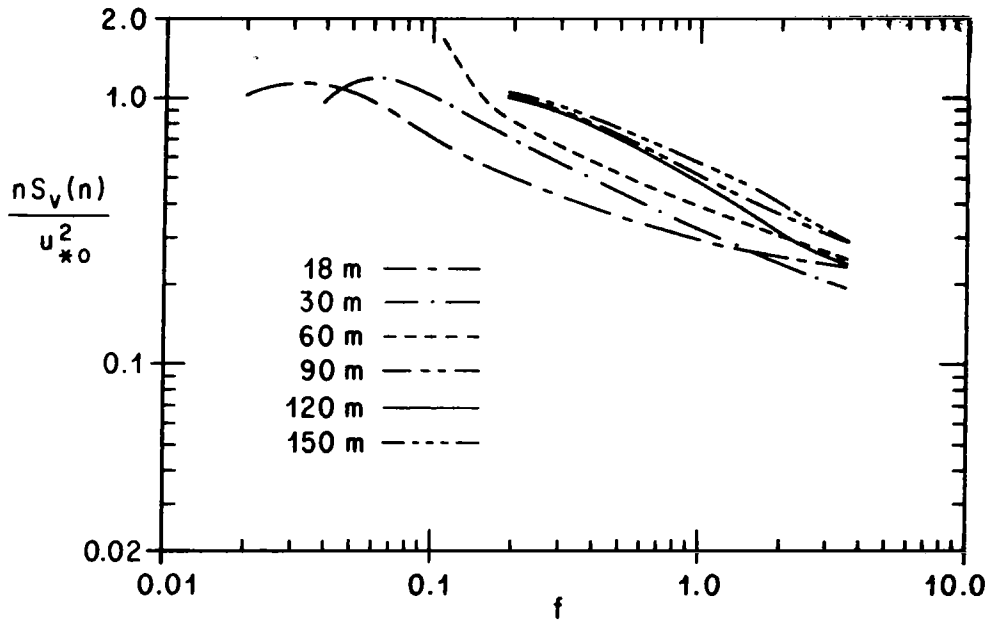


Figure 14. Dimensionless logarithmic lateral spectra for unstable wind conditions.

equally valid for the unstable case. The functions f_{mu} , f_{mv} , β_u , β_v are depicted in Figures 15 and 16, and the functions $nS_u(n)/\beta_u u_*^2$ and $nS_v(n)/\beta_v u_*^2$ are given in Figure 17. Table 1 summarizes the spectral properties of turbulence for unstable and neutral conditions.

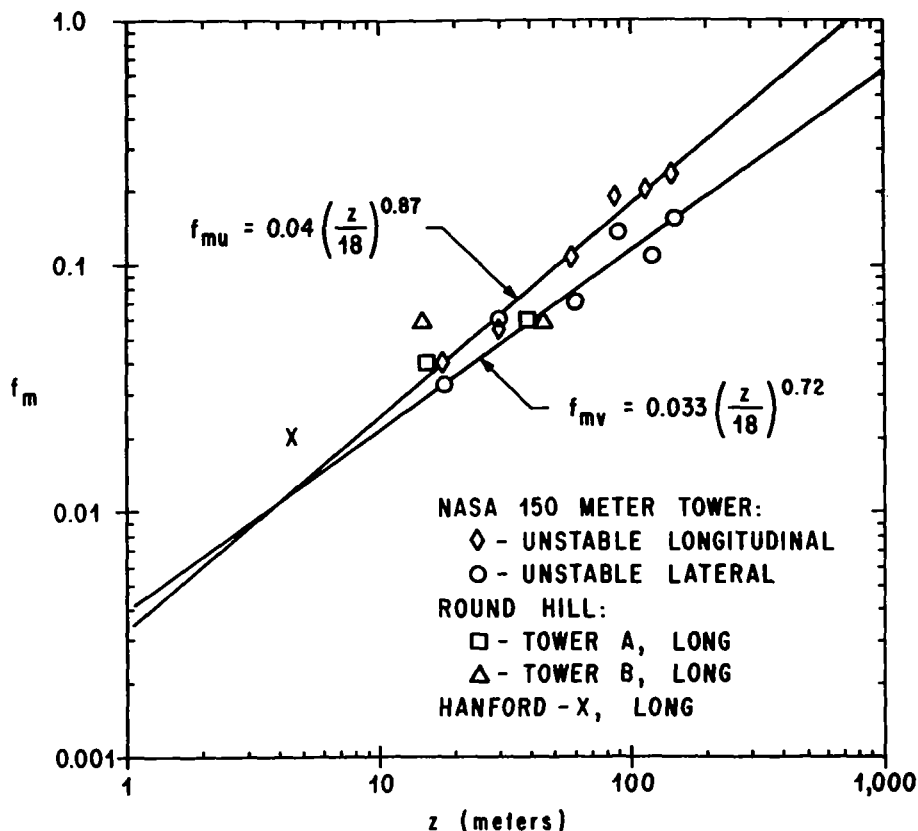


Figure 15. Vertical distributions of the dimensionless frequencies f_{mu} and f_{mv} associated with the peaks of the logarithmic longitudinal and lateral spectra for unstable wind conditions.

THE LONGITUDINAL AND LATERAL CORRELATION FUNCTIONS

The normalized correlation function $R(x)$ at space lag x is related to the spectrum through the Fourier integral

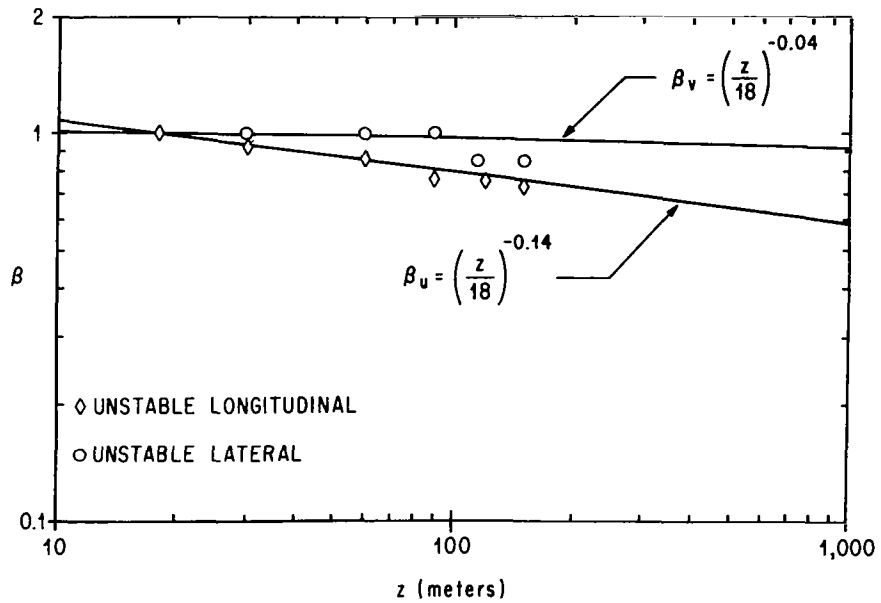


Figure 16. Vertical distributions of the collapsing factors β_u and β_v for unstable wind conditions.

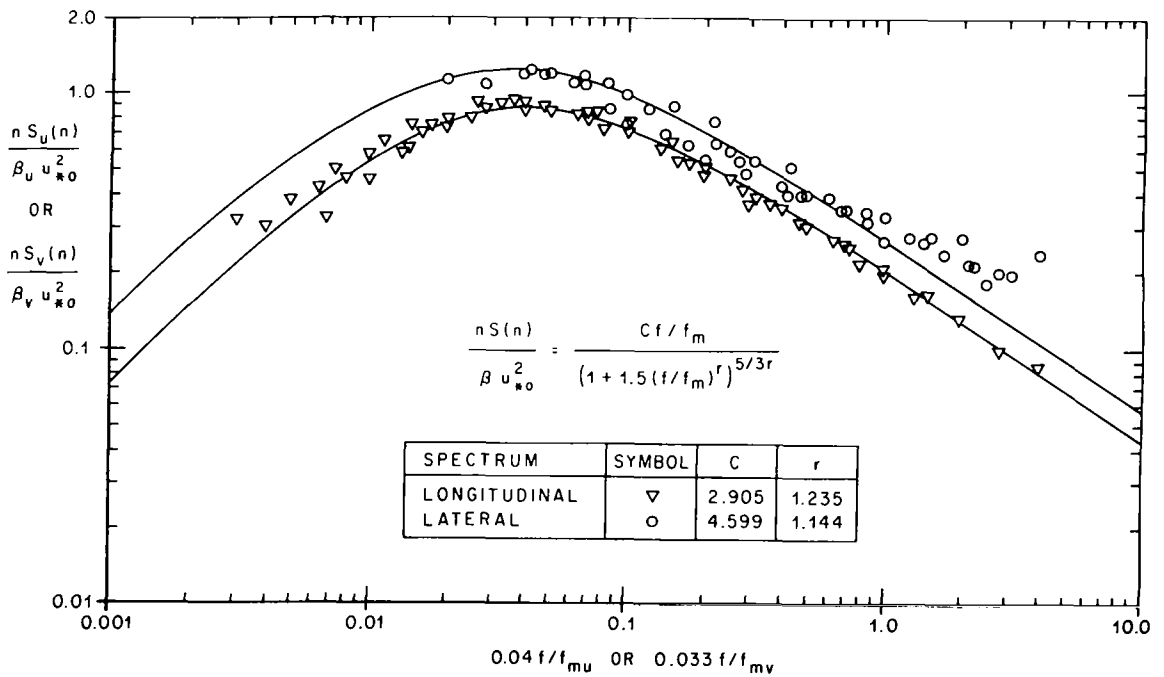


Figure 17. Dimensionless logarithmic longitudinal and lateral spectra as functions of $0.04 f/f_{\mu}$ and $0.033 f/f_{\nu}$ for unstable wind conditions.

TABLE 1. SUMMARY OF THE SPECTRAL PROPERTIES OF TURBULENCE FOR NEUTRAL AND UNSTABLE CONDITIONS

$\frac{nS(n)}{\beta u_{*0}^2} = \frac{C \frac{f}{f_m}}{\left(1 + 1.5 \left(\frac{f}{f_m}\right)^r\right)^{5/3r}}$		
	Neutral	Unstable
C_u	6.198	2.905
C_v	3.954	4.599
r_u	0.845	1.235
r_v	0.781	1.144
f_{mu}	0.03 (z/18)	0.04 (z/18) ^{0.87}
f_{mv}	0.1 (z/18) ^{0.58}	0.033 (z/18) ^{0.72}
β_u	(z/18) ^{-0.63}	(z/18) ^{-0.14}
β_v	(z/18) ^{-0.35}	(z/18) ^{-0.04}

$$\sigma^2 R(x) = \bar{u} \int_0^{\infty} S(\bar{u}\kappa) \cos(2\pi\kappa x) d\kappa, \quad (38)$$

where $\bar{u}S(\bar{u}\kappa)$ is the spectrum at wave number κ (cycles m^{-1}) and σ is the standard deviation of the turbulence. The wave number is related to the frequency through Taylor's hypothesis ($\kappa = n/\bar{u}$). Substitution of equation (33) or (34) into equation (38) yields

$$\frac{\sigma^2 R(\xi)}{\beta u_{*0}^2} = C \int_0^{\infty} \frac{\cos(2\pi\xi\zeta) d\zeta}{\left(1 + 1.5 \zeta^r\right)^{5/3r}}, \quad (39)$$

where

$$\left. \begin{aligned} \zeta &= \frac{f}{f_m} \\ \xi &= \frac{x f_m}{z} \end{aligned} \right\} \quad (40)$$

The quantity ξ is the dimensionless space lag at height z , and the integral in equation (39) is a function of ξ only. Integration of equation (39) for neutral and unstable conditions with Simpson's rule yielded the results illustrated in Figures 18 and 19.

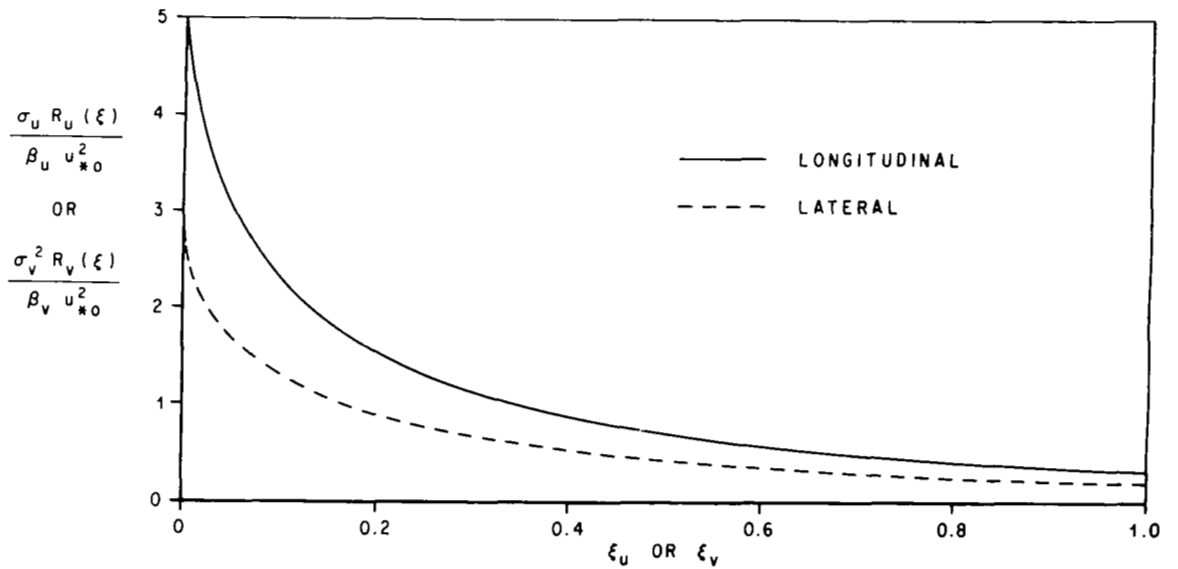


Figure 18. Scaled correlation functions for the longitudinal and lateral components of turbulence as functions of the dimensionless space lag ξ for neutral wind conditions.

The dimensionless standard deviation $\sigma/\beta^{1/2}u_{*0}$ can be obtained from equation (39) by setting $\xi = 0$ and then taking the positive square root of the resulting expression, so that

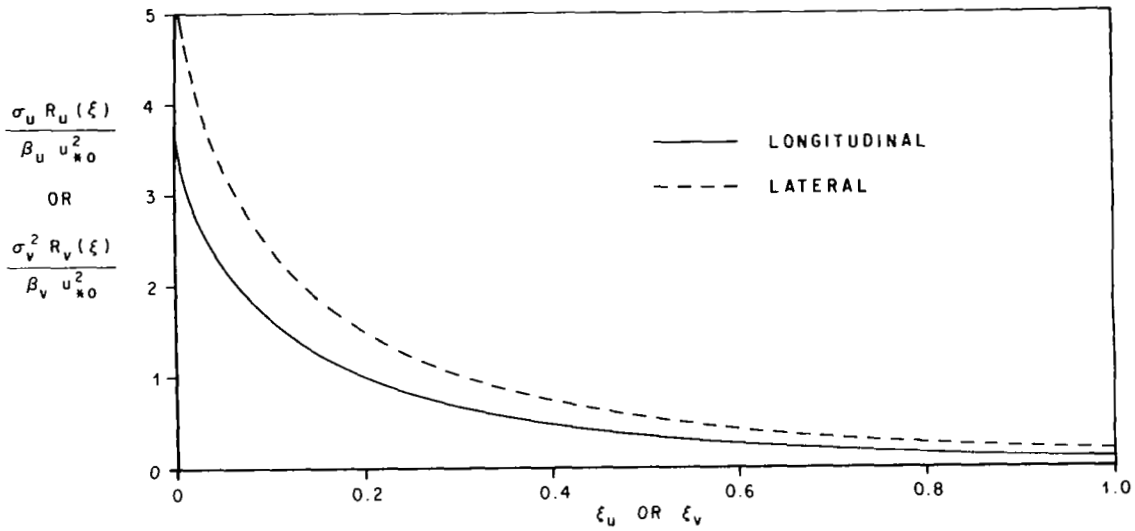


Figure 19. Scaled correlation functions for the longitudinal and lateral components of turbulence as functions of the dimensionless space lag ξ for unstable wind conditions.

$$\frac{\sigma}{\beta^{1/2} u_{*0}} = \left[C \int_0^{\infty} \frac{d\xi}{(1 + 1.5 \xi^r)^{5/3r}} \right]^{1/2} \quad (41)$$

The right side of equation (41) is a pure number, values for which can be found in Table 2.

The function

$$\frac{\sigma^2 R(\xi)}{\beta u_{*0}^2} = \frac{\sigma^2}{\beta u_{*0}^2} \left[1 + \frac{6.815}{\delta} \frac{C}{(1.5)^{5/3r}} \frac{\beta u_{*0}^2}{\sigma^2} \xi^{2/3} \right]^{-\delta} \quad (42)$$

TABLE 2. PROPERTIES OF THE CORRELATION FUNCTIONS FOR NEUTRAL AND UNSTABLE CONDITIONS

	Neutral	Unstable
$\sigma_u / \beta_u^{1/2} u_{*o}$	2.227	1.897
$\sigma_v / \beta_v^{1/2} u_{*o}$	1.677	2.302
$L_u^* f_{mu}/z$	0.282	0.188
$L_v^* f_{mv}/z$	0.332	0.199

was selected to represent the results of the numerical integrations for the neutral case. The parameter δ is determined by least-square methods. For sufficiently small values of ξ , this function behaves like

$$R(\xi) = 1 - 6.815 \frac{C}{(1.5)^{5/3r}} \frac{\beta u_{*o}^2}{\sigma^2} \xi^{2/3} \quad (43)$$

Now the theory of isotropic homogeneous turbulence predicts that, in the inertial subrange,

$$\frac{R_v(x) - 1}{R_u(x) - 1} = \frac{4}{3} \quad (44)$$

and equation (43) predicts that

$$\frac{R_v(x) - 1}{R_u(x) - 1} \rightarrow \left[\frac{C_v}{C_u} \frac{\beta_v}{\beta_u} \left(\frac{f_{mv}}{f_{mu}} \right)^{2/3} \left(\frac{3}{2} \right)^{5/3} \left(\frac{1}{r_u} - \frac{1}{r_v} \right) \right] \left(\frac{\sigma_u}{\sigma_v} \right)^2 \quad (45)$$

as $\xi \rightarrow 0$. The quantity within the brackets on the right side of equation (45) is equal to $4/3$, according to equation (35), and $\sigma_u/\sigma_v \neq 1$. The apparent inconsistency between equations (44) and (45) results because

equation (44) is based upon the entire flow being isotropic, while equation (45) is based on spectra associated with turbulent flows which are only locally isotropic in wave number space for sufficiently large wave numbers. Thus, upon producing the Fourier integral, equation (39), we obtained contributions to $R(\xi)$ from both the isotropic and anisotropic portions of the turbulent flow. The quantities

$$\delta_u = 4.758$$

$$\delta_v = 3.399$$

and the function in equation (42) reproduce the results of the numerical integrations of equation (39), for the neutral case, to within a few percent.

In the unstable case, the function given by equation (42) does not reproduce the results of the numerical integrations at large values of ξ for all values of δ . To remedy this, an exponential factor was introduced into the expression and the function

$$\frac{\sigma^2 R(\xi)}{\beta u_{*0}^2} = \frac{\sigma^2}{\beta u_{*0}^2} \left[1 + 6.815 \frac{C}{(1.5)^{5/3r}} \frac{\beta u_{*0}^2}{\sigma^2} \xi^{2/3} \right]^{-1} e^{-\lambda \xi^\gamma} \quad (46)$$

was selected to represent the results of numerical integrations for the unstable case. The quantities λ and γ are determined by least-square methods. It appears that $\gamma = 0.9$ can be used for both the longitudinal and lateral spectra and

$$\lambda_u = 2.22$$

$$\lambda_v = 2.02$$

The function given by equation (46) yields a good fit near $\xi = 0$; however, it departs from the results of the numerical integrations by approximately 10 percent at $\xi = 1$. Near the origin, equation (46) behaves like equation (43), consistent with hypothesis of the inertial subrange.

Let us now turn our attention to the longitudinal and lateral integral scales of turbulence which are defined by the expression

$$L^* = \int_0^{\infty} R(x) dx \quad . \quad (47)$$

The integral scale, defined in terms of the dimensionless space lag, is given by

$$\frac{L^* f_m}{z} = \int_0^{\infty} R(\xi) d\xi \quad . \quad (48)$$

This integral is a pure number, and upon substituting the expressions given by equations (42) and (46) for $R(\xi)$ and employing Simpson's integration rule, we obtain the results in Table 2.

Various investigators [4] have represented the correlation functions of atmospheric turbulence with the expression

$$R(x) = e^{-x/L^*} \quad . \quad (49)$$

The logarithmic spectrum associated with this expression is given by

$$\frac{nS(n)}{u_{*0}^2} = \frac{2}{\pi} \frac{\sigma^2}{u_{*0}^2} \frac{\frac{2\pi f L^*}{z}}{\left(\frac{2\pi f L^*}{z}\right)^2 + 1} \quad . \quad (50)$$

This function has a maximum value at

$$\frac{L^* f_m}{z} = \frac{1}{2\pi} = 0.159 \quad . \quad (51)$$

This value of the dimensionless integral scale is significantly less (approximately 45 percent) than the ones in Table 2 for the neutral case. However, for the unstable case, the integral scales given by equation (51) depart from the ones in Table 2 by only approximately 20 percent.

In the neutral case, f_{mu} and f_{mv} are proportional to z and $z^{0.58}$, so that L_{u}^* is a constant and L_{v}^* is proportional to $z^{0.42}$. The former is consistent with the results of Davenport's [11] analysis of high wind speed spectra. In unstable air, f_{mu} and f_{mv} are proportional to $z^{0.87}$ and $z^{0.72}$, and thus L_{u}^* and L_{v}^* are proportional to $z^{0.13}$ and $z^{0.28}$.

THE DISSIPATION RATE OF TURBULENCE

It is possible to estimate the dissipation rate of turbulence by examining the asymptote of the dimensionless logarithmic spectrum for large f values. According to equation (33), the longitudinal spectrum, for sufficiently large values of f , is asymptotically given by

$$\frac{nS_{\text{u}}(n)}{u_{*0}^2} \sim \beta_{\text{u}} \frac{C_{\text{u}}}{(1.5)^{5/3} r_{\text{u}}} \left(\frac{f}{f_{\text{mu}}} \right)^{-2/3} \quad (52)$$

Upon equating the right sides of equations (13) and (52), we obtain

$$\phi_{\epsilon} = \frac{k_1}{(1.5)^{5/2} r_{\text{u}}} \left(\frac{C_{\text{u}}}{\alpha} \right)^{3/2} \beta_{\text{u}}^{3/2} f_{\text{mu}} \quad (53)$$

According to the information given in Table 1 and equation (53), ϕ_{ϵ} in neutral air is given by

$$\phi_{\epsilon} = \left(\frac{z}{18} \right)^{0.055} \quad (54)$$

while in unstable air, it is given by

$$\phi_{\epsilon} = 0.63 \left(\frac{z}{18} \right)^{0.66} \quad . \quad (55)$$

One should keep in mind that equation (55) was derived from a spectral model, which is an average of the unstable data, so that equation (55) is probably valid for conditions associated with values of Ri on the order of -0.3 .

At $z/L = 0$ we have $\phi(0) = 1$, so that, according to either hypothesis I or II [equations (19) or (21)], we must have $\phi_{\epsilon}(0) = 1$. However, equation (54) predicts that $\phi_{\epsilon}(0) < 1$ below $z = 18$ m for the neutral case and at $z = 0$ we have $\phi_{\epsilon}(0) = 0$. Actually, the layer of air in the domain $0 < z \leq 18$ m is in the Monin layer, and we should have $\phi_{\epsilon} = 1$ throughout this layer during neutral wind conditions. If we accept a 10 percent error in ϕ_{ϵ} as a measure of the validity of the spectral representations given by equations (33) and (34), then it follows from equation (54) that the model can be extrapolated down to the 3-m level in the neutral case.

To understand the behavior of ϕ_{ϵ} in the unstable case, we write the eddy energy equation for the steady-state boundary layer in the form

$$\left(\frac{u_*}{u_{*0}} \right)^2 \phi - \frac{z}{L} - \phi_{\epsilon} - \phi_D = 0 \quad . \quad (56)$$

Let us assume that the heat flux is height-invariant, so that L is a constant. At the surface of the earth, z/L vanishes, $(u_*/u_{*0})^2 \phi(0) = 1$, and $\phi_D(0) = 0$ according to both hypotheses I and II; thus, $\phi_{\epsilon}(0) = 1$. As we proceed away from the earth into the unstable Monin layer, ϕ_D is balanced by z/L , and ϕ_{ϵ} is balanced by ϕ according to hypothesis I (in the Monin layer $u_* = u_{*0}$). Because ϕ is a decreasing function of $-z/L$, it follows that ϕ_{ϵ} is a decreasing function of z below 18 m. However, based upon an

analysis of a sample of Cape Kennedy data, Panofsky suggests that ϕ_D is unimportant in unstable air at 30 m and above. This conclusion may not be strictly true for the entire layer above 30 m, but it is reasonable to suppose that ϕ_D becomes negligibly small or vanishes somewhere above 30 m. In addition, for sufficiently large z , the dimensionless shear ϕ is small compared to $-z/L$ and $(u_*/u_{*0})^2 < 1$, so that, according to equation (56), ϕ_ϵ can be estimated as $-z/L$. Thus, at sufficiently large heights, ϕ_ϵ is an increasing function of z . Therefore, ϕ_ϵ must experience a minimum in the lower levels. Equation (55) implies that ϕ_ϵ is an increasing function of z in the unstable boundary layer [$Ri(18\text{ m}) \sim -0.3$]; therefore, the minimum in ϕ_ϵ must occur at the 18-m level if we accept hypothesis I and equation (55). The minimum in ϕ_ϵ actually occurs somewhere between the 18- and 30-m levels if the implications of hypothesis I are correct. If this minimum in ϕ_ϵ exists, it was not detected because of the wide spacing between the instrumentation levels on the tower.

The level above 30 m at which ϕ_D vanishes in the unstable model can be estimated with equation (56). Following Panofsky [14], we assume that $(u_*/u_{*0})^2\phi$ is small compared to $-z/L$; we set $\phi_D = 0$ in equation (56) and then combine the resulting relationship with equation (55) to obtain

$$-\frac{z^*}{L} = 0.63 \left(\frac{z^*}{18} \right)^{0.66}, \quad (57)$$

where z^* is the level at which ϕ_D vanishes. The 18-m level Richardson number for the mean unstable model is on the order of -0.3 . Therefore, according to equation (6), $18/L' = -0.19$. Now, $L = K_m L'/K_h$ and $K_h/K_m \approx 1.3$, so that $L = -73$ m. Substituting this value of L into equation (57) yields $z^* = 283$ m. Above this level, ϕ and ϕ_D are small and $\phi_\epsilon = -z/L$. This should be compared with equation (55), which predicts that ϕ_ϵ increases as $z^{0.66}$.

The proposed energy budget scheme for the unstable boundary layer is summarized in Figure 20. In the lowest layer, the Monin layer, the energy budget is given by hypothesis I [equation (19)]. Above this layer, there is a transition region, between approximately the 18- and 30-m levels, in which the energy budget transforms from a type I to a type III budget. A type III budget is one in which the mechanical and buoyant energy production terms and the energy flux divergence term all contribute to ϕ_ϵ to varying degrees. From the base of the transition layer to a level on the order of 300 m, ϕ and ϕ_D tend toward zero as z increases. Finally, above this level we have a region in which the buoyant energy production is balanced by the dissipation. For this scheme to work, the various functions in the energy equation must be functions of z/L and z scaled with a length scale other than L . The additional length scale should be a function of the external synoptic- and meso-scale conditions which force the turbulent flow in the boundary layer.

VERTICAL VARIATION OF STRESS IN NEUTRAL AIR

An estimate of the vertical variation of the stress in neutral air can be obtained with equation (54) and an inviscid estimate of ϵ given by

$$\epsilon = \frac{u_*^3}{L_B} \quad , \quad (58)$$

where L_B is a representative dimension of the momentum carrying eddies. In the Monin layer,

$$L_B = k_1 z \quad (59)$$

Above the Monin layer, L_B increases slower than $k_1 z$ and should approach a constant as z becomes large. In an analysis of the vertical distribution of wind in the neutral baroclinic boundary layer, Blackadar [10] points out that

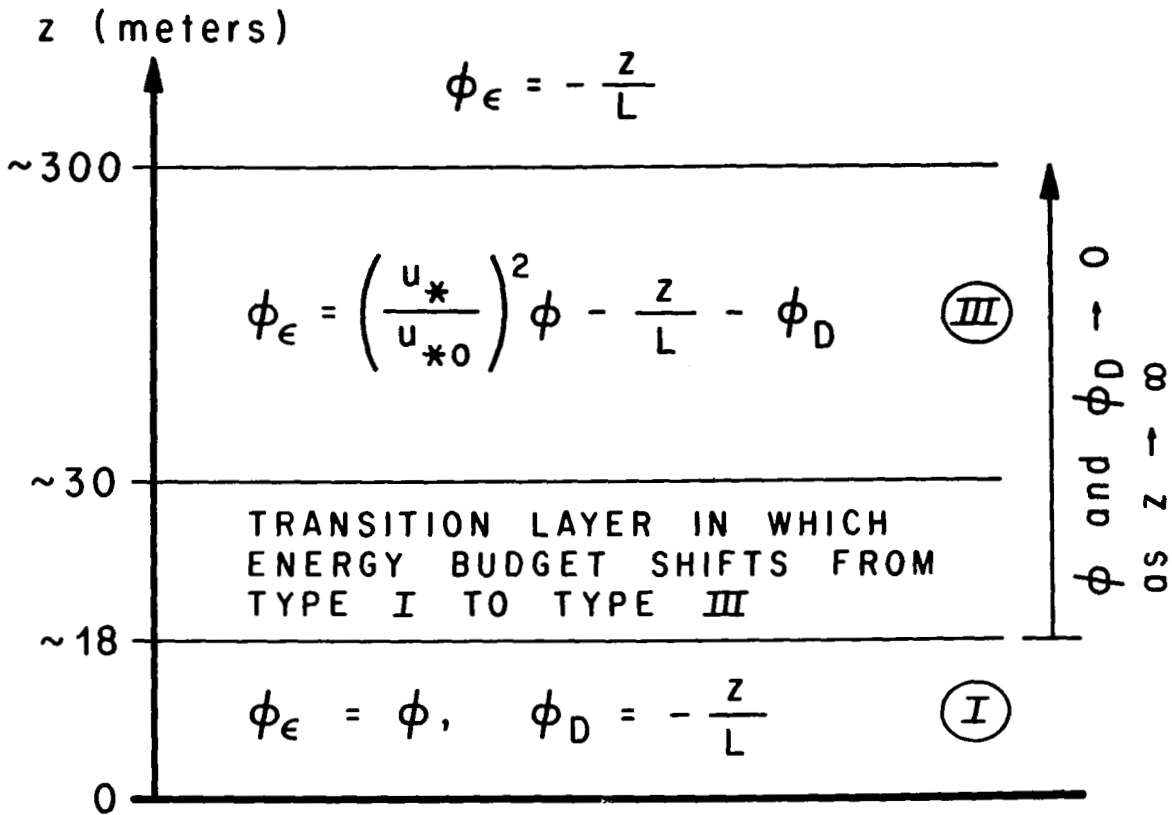


Figure 20. Hypothesized scheme of the budget of turbulent energy in the unstable boundary layer for $Ri(18\text{ m}) \approx -0.3$.

$$L_B = \frac{k_1 z}{k_1 f_c z + 1 + \frac{0.00027U}{k_1 f_c z}} \quad (60)$$

describes the few observed distributions of L_B rather well, where U is the surface geostrophic wind and f_c is the Coriolis parameter. Upon combining equations (54), (58), and (60), we find that, in the neutral boundary layer,

$$\left(\frac{u_*}{u_{*0}} \right)^2 = \frac{\left(\frac{z}{18} \right)^{0.037}}{\left[1 + \frac{k_1 f_c z}{0.00027U} \right]^{2/3}} \quad (61)$$

This function vanishes at $z = 0$ and has a maximum value at

$$\frac{z_m}{18} = 2.203 \times 10^{-6} \frac{U}{f_c} \quad (62)$$

where U and f_c have units of m sec^{-1} and sec^{-1} , respectively. At 30 deg north, $f_c = 0.728 \cdot 10^{-4} \text{ sec}^{-1}$; therefore, in the neutral boundary layer, $z_m/18 = 0.03U$. At $z = 0$ we should have $(u_{*0}/u_{*0})^2 = 1$. However, the function given by equation (61) vanishes at $z = 0$ and increases with z when $z < z_m$. Thus, this function is valid only when $z > z_m$. The data which were used to construct the neutral spectral model were generally associated with conditions in which $U < 15 \text{ m sec}^{-1}$, making $z_m < 8 \text{ m}$. Equation (61) predicts reasonable estimates of the local stress for the neutral boundary layer above 18 m. The corresponding estimate for the unstable case with Blackadar's length scale fails to give reasonable vertical variations of the stress.

CONCLUDING COMMENTS

An engineering model of the longitudinal and lateral spectra of turbulence has been developed. The analytical expressions used to represent the spectra are asymptotically consistent with a sufficiently large wave number with the well-known properties of isotropic turbulence in the inertial subrange. Based on an analysis of the longitudinal spectrum in the inertial subrange at the 18-m level, it seems that in the Monin layer the mechanical and buoyant production rates of turbulent kinetic energy are balanced by the viscous dissipation and flux divergence terms, respectively. However, since the friction velocity was not measured directly, it is not possible to be sure that the correct hypothesis of the energy budget has really been selected. The friction velocities are derived for these cases from mean wind speed and temperature profiles by the use of assumptions whose validity can only be established if the friction velocity is known. Accordingly, the proposed energy budget should be considered tentative.

The Fourier transform mates, or rather the correlation functions, associated with the spectral representations were obtained by numerical integration, and formulae were selected to represent the results of these

integrations. It is concluded from an analysis of the correlation functions that σ_u and σ_v behave like $z^{-0.315}$ and $z^{-0.175}$ in neutral air, while in unstable air they are proportional to $z^{-0.07}$ and $z^{-0.02}$. In neutral air the longitudinal integral scale of turbulence is height-invariant, while the lateral integral scale behaves like $z^{-0.42}$. In unstable air, L_u^* and L_v^* are proportional to $z^{-0.13}$ and $z^{-0.28}$, respectively.

The vertical variation of the viscous dissipation was deduced from the spectral model. In the neutral boundary layer ϕ_ϵ is proportional to $z^{0.055}$, so that ϵ is proportional to $z^{-0.945}$. In the unstable boundary layer, ϕ_ϵ is proportional to $z^{0.66}$, so that ϵ is proportional to $z^{-0.34}$.

As one proceeds upward out of the Monin layer, the energy balance seems to become more complex, because the selective energy balance that occurs in the Monin layer fails in the Ekman layer and thus the mechanical and buoyant production terms together balance the viscous dissipation and flux divergence terms. At sufficiently great heights, on the order of 300 m, it seems that we again have a selective energy balance; however, we now have a situation in which the mechanical production and flux divergence terms are small and the buoyant production is balanced by the viscous dissipation.

George C. Marshall Space Flight Center

National Aeronautics and Space Administration

Marshall Space Flight Center, Alabama 35812, July 21, 1969

933-50-02-00-62

REFERENCES

1. Kaufman, J. W., and Keene, L. F.: NASA's 150-Meter Meteorological Tower Located at Cape Kennedy, Florida. NASA TM X-53259, George C. Marshall Space Flight Center, Huntsville, Alabama, May 12, 1965.
2. Fichtl, G. H.: An Analysis of the Roughness Length Associated with the NASA 150-Meter Meteorological Tower. NASA TM X-53690, George C. Marshall Space Flight Center, Huntsville, Alabama, January 3, 1968.
3. Blackman, R. B., and Tukey, J. W.: The Measurement of Power Spectra. Dover, New York, 1958.
4. Pasquill, F.: Atmospheric Diffusion. D. van Nostrand Company, Ltd., New York, 1962.
5. Monin, A. S.: On the Similarity of Turbulence in the Presence of a Mean Vertical Temperature Gradient. J. Geophys. Res., Vol. 64, 1959, pp. 2196-2197.
6. Lumley, J. L., and Panofsky, H. A.: The Structure of Atmospheric Turbulence. John Wiley and Sons, 1964.
7. Record, F. A., and Cramer, H. E.: Turbulent Energy Dissipation Rates and Exchange Processes above a Non-homogeneous Surface. Quart. J. Roy. Meteor. Soc., Vol. 92, 1966, pp. 519-561.
8. Busch, N. E., and Panofsky, H. A.: Recent Spectra of Atmospheric Turbulence. Quart. J. Roy. Meteor. Soc., Vol. 94, 1968, pp. 132-148.
9. Berman, S.: Estimating the Longitudinal Wind Spectrum Near the Ground. Quart. J. Roy. Meteor. Soc., Vol. 91, 1965, pp. 302-317.
10. Blackadar, A. K., et al.: Flux of Heat and Momentum in the Planetary Boundary Layer of the Atmosphere. The Pennsylvania State University Mineral Industries Experiment Station, Department of Meteorology, Report under AFCRL Contract No. AF9604-6641, 1965.
11. Davenport, A. G.: The Spectrum of Horizontal Gustiness Near the Ground in High Winds. Quart. J. Roy. Meteor. Soc., Vol. 87, 1961, pp. 194-211.

REFERENCES (Concluded)

12. Pritchard, F. E., Easterbrook, C. G., and McVehil, G. E.: Spectral and Exceedance Probability Models of Atmospheric Turbulence for Use in Aircraft Design. TR AFFDL-TR-65-122, Air Force Flight Dynamics Laboratory, Research and Technology Division, Air Force Systems Command, Wright-Patterson AFB, Ohio, 1965.
13. Batchelor, G. K.: The Theory of Homogeneous Turbulence. Cambridge University Press, New York, 1953.
14. Blackadar, A. K., Dutton, J. A., Panofsky, H. A., and Chaplin, A.: Investigation of the Turbulence Wind Field Below 500 Feet Altitude at the Eastern Test Range, Florida. NASA CR-1410, National Aeronautics and Space Administration, Washington, D. C.